

2012-01-01

# Multi-Physics Modeling Of Induction-Based Additive Manufacturing Of Metals

Danny W. Muse

University of Texas at El Paso, dan\_and\_kim@sbcglobal.net

Follow this and additional works at: [https://digitalcommons.utep.edu/open\\_etd](https://digitalcommons.utep.edu/open_etd)



Part of the [Computer Engineering Commons](#), and the [Electrical and Electronics Commons](#)

---

## Recommended Citation

Muse, Danny W., "Multi-Physics Modeling Of Induction-Based Additive Manufacturing Of Metals" (2012). *Open Access Theses & Dissertations*. 912.

[https://digitalcommons.utep.edu/open\\_etd/912](https://digitalcommons.utep.edu/open_etd/912)

This is brought to you for free and open access by DigitalCommons@UTEP. It has been accepted for inclusion in Open Access Theses & Dissertations by an authorized administrator of DigitalCommons@UTEP. For more information, please contact [lweber@utep.edu](mailto:lweber@utep.edu).

MULTI-PHYSICS MODELING OF INDUCTION-BASED ADDITIVE  
MANUFACTURING OF METALS

DANNY W. MUSE

Department of Electrical and Computer Engineering

APPROVED:

---

Eric W. MacDonald, Ph.D., Chair

---

Ryan B Wicker, Ph.D.

---

John A. Moya, Ph.D.

---

Benjamin C. Flores, Ph.D.  
Interim Dean of the Graduate School

Copyright ©

by

Danny Wayne Muse

2012

## **Dedication**

*For Kimberli*

MULTI-PHYSICS MODELING OF INDUCTION-BASED ADDITIVE  
MANUFACTURING OF METALS

by

DANNY WAYNE MUSE, B.S.

THESIS

Presented to the Faculty of the Graduate School of

The University of Texas at El Paso

in Partial Fulfillment

of the Requirements

for the Degree of

MASTER OF SCIENCE

Department of Electrical and Computer Engineering

THE UNIVERSITY OF TEXAS AT EL PASO

August 2012

## **Abstract**

The shift towards 3D printing of functional products has provided a glimpse of the future in terms of manufacturing technologies and the creation of volumetrically complex structures made possible only through these technologies. 3D printing has emerged from the culmination of several technologies covering multiple industries and a myriad of materials. Unlike subtractive technologies such as mills, lathes and CNC machines, where material is removed from a bulk slab or billet to produce a desired part, 3D printing uses an additive layered approach to deposit material based on cross sections of the desired part. Both approaches produce parts based on 3D models created with Computer Aided Design (CAD) software such as SolidWorks®.

The advantages of an additive approach are numerous and include part geometries which are impossible with subtractive technologies, less material waste, and often significantly less energy requirements. Disadvantages include low production rates, often less than functional materials, and poor precision compared to traditional technologies. Additive processes also tend to require more specialized raw materials than do subtractive technologies. Despite the disadvantages, the growth of 3D printing is driven by market demand from business sectors such as aerospace, medicine, automotive, and consumer electronics, and there is a strong industry effort to address the short-comings of the additive approach.

Materials for the 3D printing of functional parts fall primarily in two categories: polymers and metals. For polymers, Selective Laser Sintering (SLS), Stereolithography (SL), and Fused Deposition Modeling (FDM) are the most common 3D printing technologies. For printed metals, Electron Beam Melting (EBM®), Laser Engineered Net Shaping (LENS®), and Direct Metal Laser Sintering (DMLS) are the most common. 3D Metals machines tend to be extremely expensive and are typically found only in well-funded research centers, defense contractor R&D departments, and government laboratories. Since the strength of the U.S. economy has been shown to be largely dependent on the success of small businesses, there is clearly a need for a lower cost entry level technology that will enable competitive 3D metals processing by common machine shops and parts fabrication facilities. The work presented in this thesis is focused on basic modeling of a proposed induction-based technology for metals printing that shows promise for a lower cost system that could see widespread use

in machine shops around the world. Induction heating involves the creation of intense resonant magnetic fields which induce alternating eddy currents within conductive materials found in close proximity. These induced eddy currents produce Joule heating within the conductive body proportional to the material's temperature-dependent resistivity and the square of the frequency-dependent current density. The use of induction technology for heating and even melting metals has been around for nearly a century. The basic principle behind induction heating was discovered by Michael Faraday nearly two centuries ago [1,2]. The concept proposed in this thesis involves adapting and controlling induction heating technology to heat metal alloy filaments to a point between the solidus and liquidus states (a semi-solid state) whereby the metal filament becomes soft and can be laid down in a predictable, well-behaved manner and then be brought to a low melting point for consolidation with previously deposited layers. The thesis covers an introduction to the basics of induction heating including historical contributions and a discussion of relevant theory from electromagnetics and thermodynamics. Relevant numerical methods are presented, along with some initial ideas about applying the technology to an additive deposition process.

## Table of Contents

Abstract.....	v
List of Tables .....	ix
List of Figures.....	x
Chapter 1: Introduction.....	1
1.1    3D Printing of Metals .....	1
1.1.1 Direct Metal Laser Sintering (DMLS).....	1
1.1.2 Electron Beam Melting (EBM®) .....	3
1.1.3 Laser Engineered Net Shaping (LENS®).....	5
Chapter 2: Induction Heating Technology .....	7
2.1    A Brief History of Induction Heating.....	7
Chapter 3: Review of Physics Relevant to Induction Heating .....	13
3.1    Electromagnetics.....	13
3.2    Thermodynamics .....	19
Chapter 4: Numerical Modeling .....	22
4.1    Limitation of Scope .....	22
4.2    Numerical Method.....	23
4.2.1 Finite Element Analysis using the Galerkin method .....	24
4.2.2 Discretization of the problem domain .....	27
4.2.3 Establishment of the Global Stiffness Matrix.....	29
4.2.3 Enforcement of Boundary Conditions .....	29
4.2.4 Solution to the Matrix Equation and Post Processing .....	30
4.3    Solution to the Electromagnetic Problem .....	30
4.4    Solution to the Thermodynamic Problem.....	33
Chapter 5: Initial System Design.....	39
5.1    Off-The-Shelf Equipment.....	40
5.2    Example Load Coil Design.....	41
5.3    Soft Magnetic Composites.....	43
5.4    Coil Fabrication .....	44
5.4    Control System .....	45



Chapter 6: Future Work .....	46
6.1 Numerical Modeling of the Coupled Electro-thermal Phenomenon .....	46
6.2 Experimentation.....	47
6.3 Material Science .....	47
References.....	48
Vita .....	49

## List of Tables

<b>Table 3.1</b>	Units for electromagnetic quantities .....	15
<b>Table 3.2</b>	Units for thermodynamic quantities .....	20

## List of Figures

Figure 1.1: DMLS System from EOS.....	2
Figure 1.2: DMLS Process Schematic.....	2
Figure 1.3: Parts Fabricated with Direct Metal Laser Sintering.....	3
Figure 1.4: Arcam Electron Beam Melting (EBM®) Machine.....	3
Figure 1.5: Major Components of EBM® System.....	4
Figure 1.6: Parts fabricated with Arcam EBM® System.....	4
Figure 1.7: LENS® System in action.....	5
Figure 1.8: OPTOMECH LENS® System.....	6
Figure 1.9: Parts fabricated with LENS® technology.....	6
Figure 2.1: Hans Christian Oersted.....	8
Figure 2.2: Oersted's experiment [4].....	8
Figure 2.3: André-Marie Ampère.....	9
Figure 2.4: Ampère's discovery of electrodynamic forces.....	9
Figure 2.5: Michael Faraday.....	10
Figure 2.6: Heinrich Lenz.....	11
Figure 2.7: James Prescott Joule.....	11
Figure 2.8: James Clerk Maxwell.....	12
Figure 4.1: 2D Discretized problem domain.....	27
Figure 4.2: Refined mesh showing material boundaries.....	28
Figure 4.3: Magnetic Vector Potential with magnetic plate and Dirichlet Boundary conditions.....	31
Figure 4.4: Magnetic Vector Potential with magnetic plate and Neumann Boundary conditions.....	32
Figure 4.5: Magnetic Vector Potential with paramagnetic plate and Dirichlet Boundary conditions.....	32
Figure 4.6: Magnetic Vector Potential with paramagnetic plate and Neumann Boundary conditions.....	33
Figure 4.7: Preheated plate, no Joule Heating.....	34
Figure 4.8: Plate heat with 2 seconds of Joule Heating.....	35
Figure 4.9: Plate heat with 5 seconds of Joule Heating.....	36
Figure 4.10: Plate heat with 8 seconds of Joule Heating.....	37
Figure 4.11: Plate heat with 10 seconds of Joule Heating.....	38
Figure 5.1: Cross-section of induction coil concept.....	40
Figure 5.2: 3D model of multi-turn load coil.....	42
Figure 5.3: Photo Rendering of a Multi-turn Load Coil.....	42
Figure 5.4: Photo rendering of custom concentrator.....	43
Figure 5.5: Induction Coil with integrated concentrator.....	43
Figure 5.6: Copper load coil parts after CNC process.....	44
Figure 5.7: Coil Assembly before brazing.....	44
Figure 5.8: Completed test coil with concentrator.....	45

## **Chapter 1: Introduction**

### **1.1 3D Printing of Metals**

There is an increasing demand for complex parts made with such materials as titanium and aluminum and exotic alloys such as Inconel and Ti6Al4V. The high cost of producing these parts with traditional fabrication technologies has forced a response from the additive manufacturing world. A number of new technologies have emerged that promise to revolutionize the metals processing industry by allowing complex geometries to be built with processes that are far less wasteful in terms of both materials and energy. The dominant technologies are described below. It is expected, however, that the list of additive metals technologies will grow as the manufacturing world begins to adopt their use and realize the benefits of the technologies.

#### **1.1.1 Direct Metal Laser Sintering (DMLS)**

The first of several metal powder-based systems described herein takes much of its technology from an additive polymers process called selective laser sintering (SLS) whereby polymer powders are sintered by a laser in a layered fashion to form consolidated parts. Direct Metal Laser Sintering (DMLS) employs a similar process using metal powders. Figures 1.1 and 1.2 illustrate a DMLS machine and process schematic.



Figure 1.1: DMLS System from EOS.

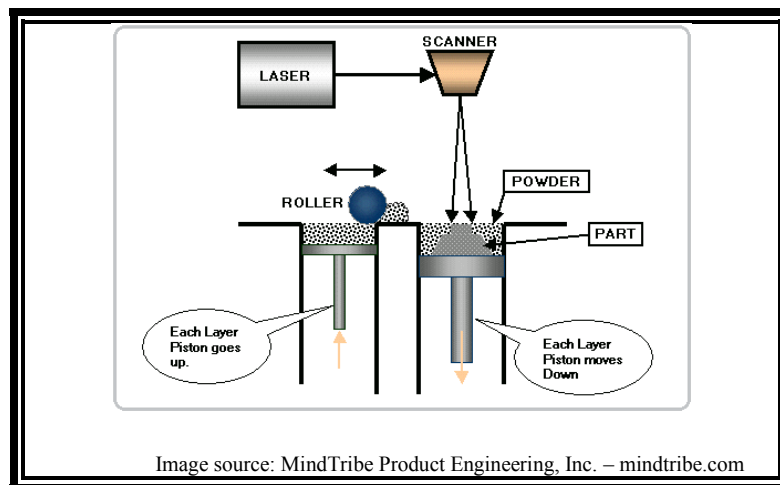


Figure 1.2: DMLS Process Schematic.

Based on a 3D model, cross-section slices are created that define the laser scan for each layer of the part. The laser system utilizes mirrors to scan this cross-section onto a metal powder bed thereby consolidating the powders and binding them to previous layers. Subsequently, the build platform is moved downward, a new layer of powder is rolled over the previous, and the process repeats until the part is complete. To mitigate oxidation of the consolidated metal, the build chamber is purged of air and then backfilled with an inert gas such as argon. Secondary processing is often used to improve the

textured surface that is characteristic of the process. Figure 1.3 shows examples of parts created with the DMLS process.



Figure 1.3: Parts Fabricated with Direct Metal Laser Sintering.

### 1.1.2 Electron Beam Melting (EBM®)

Another metal powder-based process is that of Electron Beam Melting (EBM). A modern EBM system is shown in Fig. 1.4. As with DMLS, the EBM process involves the layered consolidation of metal powders based on a 3D model. The primary difference between the technologies is the energy source used in the consolidation. Rather than a laser, an intense electron beam is used to create a melt pool at the surface of the powder. Where laser-based systems use mirrors to deflect the laser, the EBM system uses induction coils to deflect the electron beam just as it is done in the cathode ray tubes of legacy television sets.



Figure 1.4: Arcam Electron Beam Melting (EBM®) Machine.

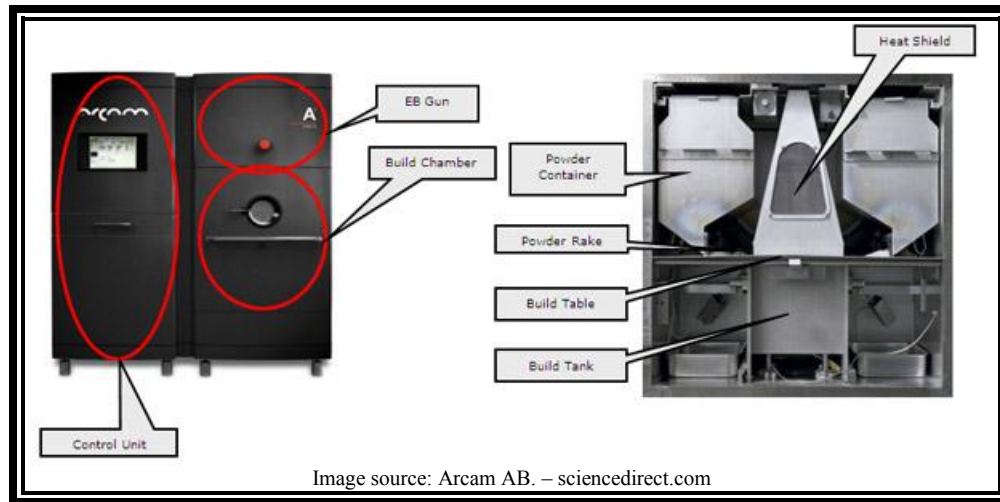


Figure 1.5: Major Components of EBM® System.

The major components of an EBM system are illustrated in Fig. 1.5. Just before the consolidation process, the electron beam is rastered across the area where a feature is being developed in order to bring the powder in that region to a temperature just below that required for melting. The beam is then vectored to follow the contours of the part based on the cross-sectional slice. This brings the powder to a melting point for consolidation. Such a process requires that the build chamber be in a high vacuum environment with an inert gas back-fill. Along with a sophisticated focusing system, this allows a very narrow electron beam since electron collisions with air molecules are virtually eliminated. This environment is also ideal for the prevention of oxidation. Like parts produced with DMLS, those of EBM have a textured surface finish that may require additional machining or polishing depending on the application. Figure 1.6 shows parts fabricated with EBM.

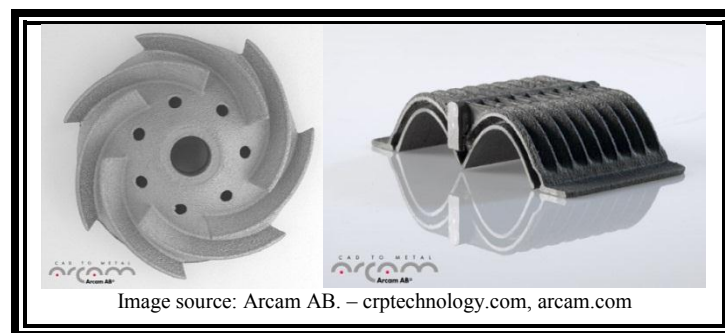


Figure 1.6: Parts fabricated with Arcam EBM® System.

### 1.1.3 Laser Engineered Net Shaping (LENS®)

The final metal powder-based technology described has a unique powder delivery system. Rather than having metal powder rolled or raked over previously consolidated layers, the Laser Engineered Net Shaping (LENS) system utilizes a unique powder jet process shown in figure 1.7. Jets of inert gas filled with the metal powders are directed to the melt zone through special nozzles (four nozzles are shown in use). As with DMLS, the energy source for the LENS system is a high powered laser.

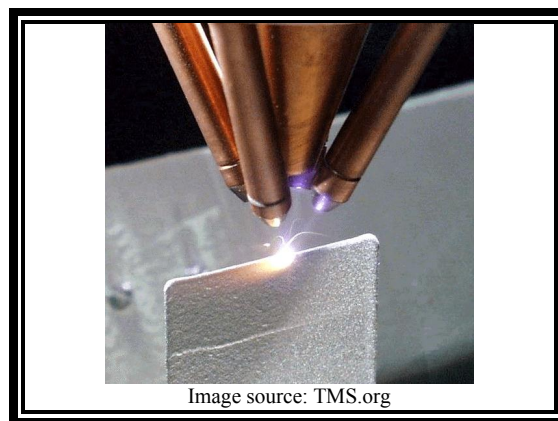


Figure 1.7: LENS® System in action.

In contrast to the other technologies described, the LENS system uses motion control hardware to translate the laser optics and powder delivery system (or the build platform upon which the part is produced) to enable the 3D layered build process. The LENS system is unique in another way compared to other powder processes in that it can be used to repair metal parts under certain conditions. As shown in Fig. 1.8, it also allows noninvasive access to the build chamber with an integrated glove box not seen in the other technologies. The LENS system is capable of producing very detailed parts as shown in Fig. 1.9.





Figure 1.8: OPTOMECH LENS® System.

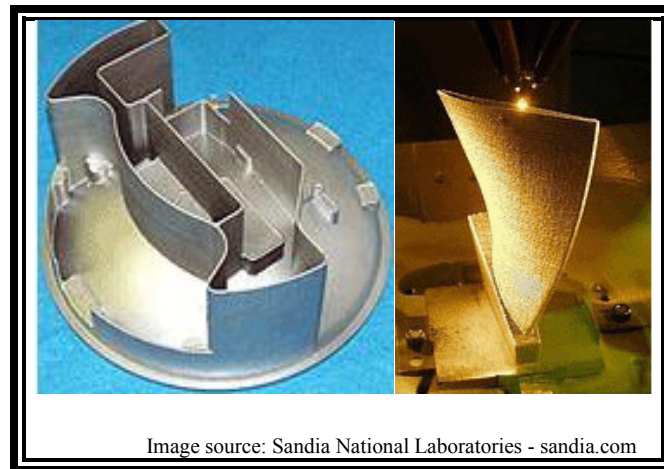


Figure 1.9: Parts fabricated with LENS® technology.

## **Chapter 2: Induction Heating Technology**

The technologies described in the previous chapter are revolutionary in that they can produce highly detailed parts with a growing range of diverse materials. Furthermore, the additive nature of these processes enables creation of volumetrically complex parts that are not possible with traditional fabrication processes. This will have a profound impact on the way engineers think about mechanical design and fabrication of feature-rich metal components. Ultimately, products and systems will benefit from this and contribute to the next industrial revolution. While the arguments for these systems are compelling, there is room to expand the available technologies and provide access to additive manufacturing to the general masses. In general, systems like those described above are likely to remain out of reach for the metal fabrication industry for some time to come. A technology is needed that can provide the basic benefits of additive manufacturing at a cost that makes it accessible to more than just the well-funded research laboratory or defense contractor. One such system might be possible by making use of a technology that has been around for more than a century, and is based on physical theory that is well understood.

Induction heating has found applications in many areas of science from metallurgy to the life sciences. Common applications include annealing, brazing, and forging, and melting. The concept presented in the remainder of this thesis is related the rapid heating of metal filaments through induction heating for layered deposition.

### **2.1 A Brief History of Induction Heating**

Any great achievement in science begins with the curiosity of a few imaginative people and their desire to understand the mysterious behavior of the world around us. Events leading to the practical use of induction heating are no different in that fundamental research in electricity and magnetism have led to revolutionary ideas, and in fact changed the world as we know it today. In 1820, Danish physicist Hans Christian Oersted, shown in Fig. 2.1, is credited with making the first observation showing a connection between electricity and magnetism while preparing for a lecture at the University of Copenhagen [1,2,4]. He discovered, some say by accident, that current flowing through a conductive

wire causes a deflection in the needle of a nearby compass. Figure 2.2 illustrates the experimental setup that Oersted used when making this discovery.

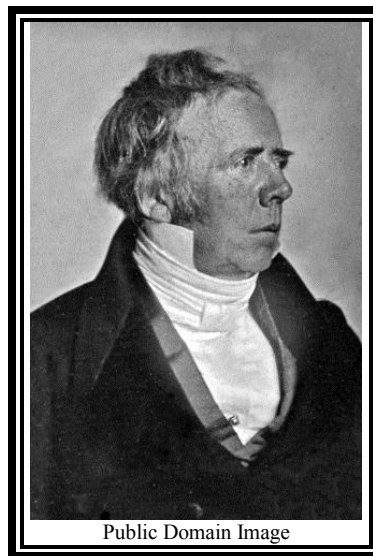


Figure 2.1: Hans Christian Oersted.

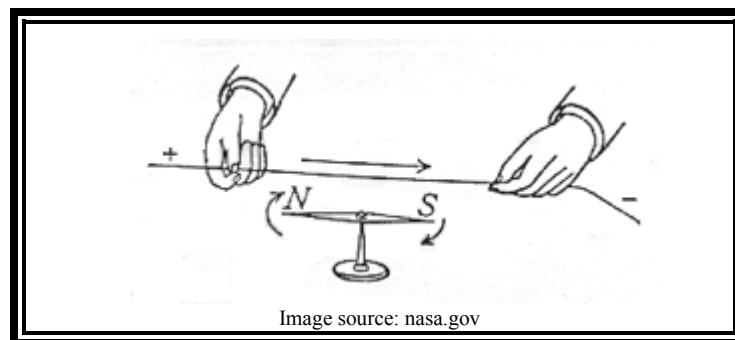


Figure 2.2: Oersted's experiment [4].

Soon after word of Oersted's discovery began spreading, French physicist and mathematician Andre-Marie Ampere, shown in Fig. 2.3, began work to develop a theory explaining the phenomenon [5]. Ampere constructed his own experiments and showed that dynamic forces were involved when individual wires carrying current were in close proximity to each other. As illustrated in Fig. 2.4, he discovered that when two wires having current flowing in the same direction were brought in close

proximity, they were attracted to each other, and when the currents were in opposite directions, the wires were repelled from each other.



Figure 2.3: André-Marie Ampère.

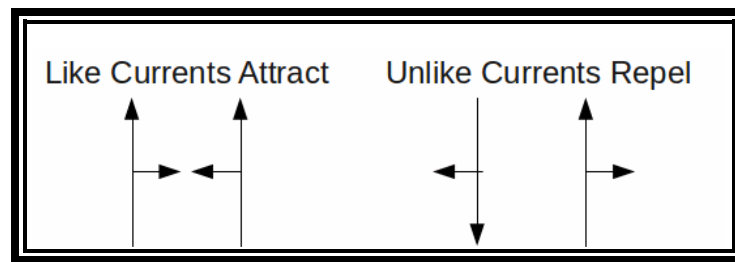


Figure 2.4: Ampère's discovery of electrodynamic forces.

Ampère also surmised that all magnetic phenomena were due to electrical currents, including what was then referred to as molecular currents inside magnetic materials [5]. We know this today as being the result of electron spin around atoms within the material. Soon after, Ampère had developed a complete theory about electrodynamics and formulated what we know as Ampère's Law.

In contrast to Oersted's discovery of magnetic fields created by electrical current through a conductor, an English scientist named Michael Faraday, shown in Fig. 2.5, studied the reverse effect [1,2]. In 1831, he found that when a magnet was moved close to a closed loop of wire, a brief current was induced in the wire. When the magnet was removed from the loop, he observed that another brief current was induced. Another experiment involved two coils of wire wrapped around a common iron

core [2]. He noticed that when a battery was connected to one of the coils, a momentary current was measured in the other coil. When the battery was removed from the first coil, he then noticed another momentary current, this time in the reverse direction. Continued experiments led Faraday to formulate the theory of electromagnetic induction. We know this formally as Faraday's Law of Induction.

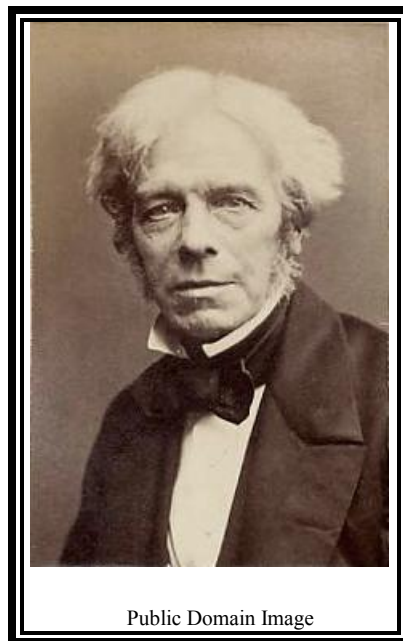


Figure 2.5: Michael Faraday.

While Faraday's discovery was an important contribution to electromagnetics, he was incorrect in his original theory in that he surmised that the induced current from his experiments flowed in the same direction as the driving current in the primary coil [1,2]. It was German physicist Heinrich Lenz shown in Fig. 2.6 who, soon after Faraday's formulation, corrected this theory by showing that the current actually flowed in the reverse direction. Lenz showed that induced current was always in a direction that opposed the change in magnetic flux that arises from a time varying source current. This is known as Lenz' Law and the law of electromagnetic induction is often referred to as the Faraday-Lenz Law as a result of this correction.

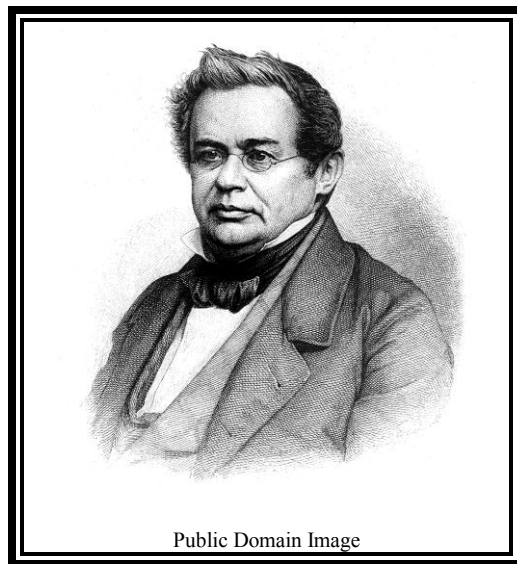


Figure 2.6: Heinrich Lenz.

As the study of electromagnetism grew, so did the interest in the heat generated by current flowing through conductive wires. Before practical applications of this electrical heating could be made, the theory behind it had to be explained. Another English physicist, James Prescott Joule, shown in Fig. 2.7, did just that when, in 1840, he formulated the law of electric heating [2]. Joule's law states that the amount of heat generated in a conductor is proportional to the resistance of the material and the square of the current flowing through it.

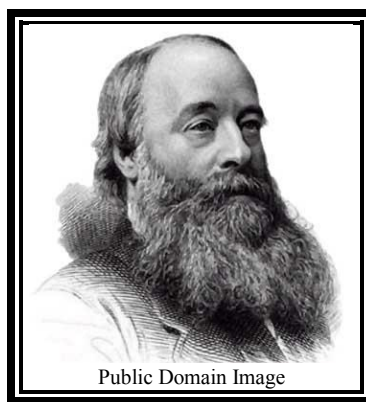


Figure 2.7: James Prescott Joule.

With the basic framework in place to discuss induction heating, credit must be given to Scottish physicist James Clerk Maxwell (Fig. 2.8) for unifying the theories of electromagnetic phenomena [2]. Maxwell made his own contribution to theory by correcting Ampere's law to account for displacement current. He was then the first in history to express the theories presented here and those of Gauss in a unified way that completely describes electromagnetic phenomena. An extraordinary result of this unification was the prediction of propagating electromagnetic waves which led to many other great accomplishments in science and engineering.

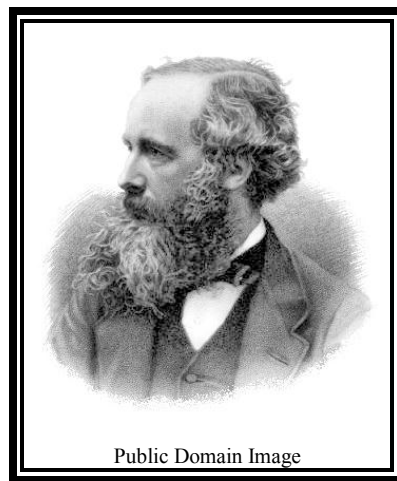


Figure 2.8: James Clerk Maxwell.

## Chapter 3: Review of Physics Relevant to Induction Heating

A good understanding of induction heating requires the study of several areas of physics. For practical reasons this paper is focused solely on the electro-thermal problem. Electromagnetics comes into play when describing the use of an alternating current source in the generation of intense magnetic fields which, in turn, induce eddy currents in nearby conductive bodies. The eddy currents penetrate conductive bodies based on the skin effect, which describes the depth at which current density drops to approximately  $1/e$  or 37% of the current at the surface of the body [12]. These induced currents cause local heating in the bodies proportional to the square of current density and the resistivity of the material. This is known as *Joule heating*. Aside from generating eddy currents in conductive bodies, alternating magnetic fields interact with bodies (conductive or not) which have a high relative magnetic permeability. The magnetic permeability of a material arises from the averaged effect of electron spin from atoms in the material and the resulting magnetic moments. When in the presence of an external time-harmonic magnetic field, work is done to align these magnetic moments throughout the body with the external fields. This work generates heat in the material proportional to the area of the hysteresis loop of the material [3]. This heating is generally called *hysteresis heating*. Another loss mechanism occurs within magnetic materials in conjunction with eddy current and hysteresis effects. These anomalous losses contribute to total losses and overall heating in a material; however, their contribution is typically negligible below radio frequencies [3]. The focus of the current study is the rapid heating of paramagnetic aluminum alloys which do not exhibit the effects of hysteresis heating or anomalous losses, therefore, the theory for these will not be covered in detail. A review of basic thermodynamics is necessary to describe what happens to these bodies when subjected to Joule heating. For both the electromagnetics and thermodynamics, the materials considered are linear, homogeneous and isotropic.

### 3.1 Electromagnetics

There are several ways to approach the eddy current problem. One common and fairly straightforward approach is to solve for the magnetic vector potential ( $\vec{A}$ ) throughout the problem domain and then solve for eddy current density ( $\vec{J}_e$ ) and Joule-effect heat source from the potential



during post-processing. Finding a suitable differential equation in terms of the magnetic vector potential requires examination of Maxwell's equations for electromagnetic phenomenon (particularly Faraday's law and Ampere's law) along with the constitutive relations which work in conjunction with Maxwell's equations to describe the interactions of fields and waves with materials.

**Maxwell's equations in differential form describing electromagnetic phenomena:**

$$\nabla \cdot \vec{D} = \rho_v \quad \text{Gauss' Law for electric fields} \quad (1)$$

$$\nabla \cdot \vec{B} = 0 \quad \text{Gauss' Law for magnetic fields} \quad (2)$$

$$\nabla \times \vec{E} = -j\omega\vec{B} \quad \text{Faraday's Law} \quad (3)$$

$$\nabla \times \vec{H} = \vec{J} + j\omega\vec{D} \quad \text{Ampere's Law} \quad (4)$$

Constitutive Relations:

$$\vec{D} = [\varepsilon]\vec{E}. \quad (5)$$

$$\vec{B} = [\mu]\vec{H}. \quad (6)$$

$$\vec{J} = [\sigma]\vec{E}. \quad (7)$$

**Table 3.1** Units for electromagnetic quantities

$\vec{D}$	Charge Displacement	$\frac{\text{Coulombs}}{m^2}$
$\vec{E}$	Electric Field Intensity	$\frac{\text{Volts}}{m}$
$\vec{B}$	Magnetic Flux density	$\frac{\text{Webers}}{m}$
$\vec{H}$	Magnetic Field Intensity	$\frac{\text{Amperes}}{m}$
$\vec{J}$	Current Density	$\frac{\text{Amperes}}{m^2}$
$\epsilon$	Dielectric Permittivity	$\frac{\text{Farads}}{m}$
$\mu$	Magnetic Permeability	$\frac{\text{Henries}}{m}$
$\sigma$	Electric Conductivity	$\frac{\text{Siemens}}{m}$
$\rho_v$	Volumetric Charge Density	$\frac{\text{Coulombs}}{m^3}$
$\omega$	Radian Frequency ( $2\pi f$ )	$\frac{\text{Radians}}{\text{second}}$

The following derivation of equation (21) for the magnetic vector potential is assembled from various sections found in [3]. The magnetic vector potential ( $\vec{A}$ ) is related to ( $\vec{B}$ ) through

$$\vec{B} = \nabla \times \vec{A}. \quad (8)$$

Equation (8) satisfies the divergence requirement in (2) since the divergence of the curl of any vector field is zero. Since we are not concerned with propagating electromagnetic waves, and since the problem domain is very small compared to a wavelength, we can neglect the displacement current term ( $j\omega\vec{D}$ ) in (4) [7,9,12]. Then current density ( $\vec{J}$ ) is related to ( $\vec{H}$ ) through

$$\vec{J} = \nabla \times \vec{H}. \quad (9)$$

From (9) and using the relation in (6),

$$\nabla \times \frac{1}{\mu} \vec{B} = \nabla \times \frac{1}{\mu} (\nabla \times \vec{A}) = \vec{J}. \quad (10)$$

Total current density includes source current and induced eddy currents.

$$\vec{J}_T = \vec{J}_s + \vec{J}_e. \quad (11)$$

Induced eddy currents are the result of an induced electric field within a conductive body.

$$\vec{J}_e = \sigma \vec{E}. \quad (12)$$

The time domain expression for Faraday's Law is

$$\nabla \times \vec{E}(t) = -\frac{\partial \vec{B}(t)}{\partial t}. \quad (13)$$

Substituting (8) into this expression leads to

$$\nabla \times \vec{E}(t) = -\frac{\partial}{\partial t} (\nabla \times \vec{A}(t)),$$

$$\nabla \times \vec{E}(t) + \left( \nabla \times \frac{\partial}{\partial t} \vec{A}(t) \right) = 0,$$

$$\nabla \times (\vec{E}(t) + \frac{\partial}{\partial t} \vec{A}(t)) = 0,$$

$$(\nabla \times)^{-1} \nabla \times (\vec{E}(t) + \frac{\partial}{\partial t} \vec{A}(t)) = (\nabla \times)^{-1} (0),$$

$$\vec{E}(t) + \frac{\partial}{\partial t} \vec{A}(t) = 0. \quad (14)$$

It follows that eddy current density ( $\vec{J}_e$ ) is related to the magnetic vector potential ( $\vec{A}$ ) by

$$\begin{aligned} \vec{E}(t) &= -\frac{\partial \vec{A}}{\partial t}, \\ \vec{J}_e(t) &= -\sigma \frac{\partial \vec{A}}{\partial t}. \end{aligned} \quad (15)$$

From (11) and (15) total current density ( $\vec{J}_T$ ) becomes

$$\vec{J}_T = -\sigma \frac{\partial \vec{A}}{\partial t} + \vec{J}_s. \quad (16)$$

Modifying (10) to account for eddy currents,

$$\nabla \times \frac{1}{\mu} (\nabla \times \vec{A}) - \sigma \frac{\partial \vec{A}}{\partial t} + \vec{J}_s = 0. \quad (17)$$

With linear materials and a known source current, we have a second order differential equation with the only unknown being the magnetic vector potential ( $\vec{A}$ ). Equation (17) is valid for any type of source current and for both linear and nonlinear materials. It should be noted, however, that when nonlinear materials are considered, permeability ( $\mu$ ) becomes a function of magnetic flux density ( $\vec{B}$ ) and the equation must be solved iteratively based on the B(H) curve of the material [3,13]. If the source current is sinusoidal and linear materials are used then a steady state frequency domain solution is

possible [3]. In this case, the magnetic vector potential becomes complex and equation (17) can be modified as follows:

$$\nabla \times \frac{1}{\mu} (\nabla \times \vec{\tilde{A}} e^{j\omega t}) - \sigma \frac{\partial}{\partial t} (\vec{\tilde{A}} e^{j\omega t}) + \vec{J}_s e^{j\omega t} = 0, \quad (18)$$

where  $\vec{\tilde{A}} = \vec{A} e^{j\alpha}$ , and  $(\alpha)$  is the phase angle between the source and the complex magnetic vector potential. For a single source, this phase angle can be approximated as zero. Applying the derivative on the second term in (18) and factoring out the complex exponential term results in

$$\nabla \times \frac{1}{\mu} (\nabla \times \vec{\tilde{A}}) - \sigma j\omega \vec{\tilde{A}} + \vec{J}_s = 0. \quad (19)$$

Now to put this expression in terms that are convenient for numerical modeling of the 2D case, we expand the first term as follows:

$$\nabla \times \frac{1}{\mu} (\nabla \times \vec{\tilde{A}}) = \frac{\partial}{\partial x} \frac{1}{\mu} \frac{\partial \vec{\tilde{A}}}{\partial x} + \frac{\partial}{\partial y} \frac{1}{\mu} \frac{\partial \vec{\tilde{A}}}{\partial y} = \nabla \cdot \left( \frac{1}{\mu} \nabla \vec{\tilde{A}} \right) \quad (20)$$

Substituting (20) into (19) yields

$$\nabla \cdot \left( \frac{1}{\mu} \nabla \vec{\tilde{A}} \right) - \sigma j\omega \vec{\tilde{A}} + \vec{J}_s = 0. \quad (21)$$

With proper boundary conditions imposed, the solution to this second order differential equation provides the complex magnetic vector potential at all points in the problem domain. From this result, instantaneous eddy current density can be calculated in regions where conductive materials exist and a non-zero magnetic vector potential is present.

$$\vec{J}_e(t) = \text{Re}(-\sigma j\omega \vec{\tilde{A}} e^{j\omega t}). \quad (22)$$

In the 2D case,  $(\vec{J}_e)$  and  $(\vec{A})$  have components only in the ‘z’ direction. With sinusoidal source current and linear materials, average eddy current density is then

$$J_{e(avg)} = \frac{(J_e(t)|_{t=0})}{\sqrt{2}} = \frac{Re(-\sigma j\omega \vec{A})}{\sqrt{2}}. \quad (23)$$

The Joule heat source is

$$Q = \int \frac{(J_{e(avg)})^2}{\sigma} ds, \quad (24)$$

where  $(S)$  is the cross-sectional area and  $(\sigma)$  is the electrical conductivity in that area. As a final note, AC current density decreases exponentially from its value at the surface based on the depth from the surface as follows [7,12 ]:

$$J = J_s e^{-d/\delta}, \quad (25)$$

where  $(J_s)$  is current density at the surface of the conducting body,  $(d)$  is the depth from the surface, and  $(\delta)$  is the *skin depth* defined as

$$\delta = \sqrt{\frac{2}{\omega \sigma \mu}}, \quad (26)$$

### 3.2 Thermodynamics

The basic thermodynamic problem related to induction heating involves the transfer of heat. There are three mechanisms for heat transfer: conduction, convection, and radiation.

**Table 3.2** Units for thermodynamic quantities

T	Temperature (Kelvin)	$K$
$\rho$	Material mass density	$\frac{g}{m^3}$
$c_m$	Mass specific heat capacity	$\frac{W}{gK}$
$c_v$	Volumetric specific heat capacity	$\frac{W}{m^3K}$
k	Thermal Conductivity	$\frac{W}{mK}$
h	Coefficient of convection heat transfer	$\frac{W}{m^2K}$
$\varepsilon$	Emissivity of the radiating body	unitless
$\gamma$	Stephan-Boltzmann constant	$\frac{W}{m^2K^4}$
Q	Volumetric power density	$\frac{W}{m^3}$
$\vec{\phi}_q$	Heat flux	$\frac{W}{m^2}$

Conduction is described by the heat conduction equation [6,8,10,11,14]:

$$\rho c_m \frac{\partial T}{\partial t} + \nabla \cdot (-k \nabla T) = Q, \quad (27)$$

where ( $\rho$ ) is the mass density of the material, ( $c$ ) is the mass specific heat capacity of the material, and ( $k$ ) is the thermal conductivity of the material. ( $Q$ ) is the volumetric heat source, and ( $T$ ) is temperature. If using a volumetric specific heat capacity ( $c_v$ ), the mass density ( $\rho$ ) is dropped from the equation. Boundary conditions for the thermal problem are related to convection and radiation, the remaining two mechanisms for heat transfer [6,8,10,11,14]. Convection is defined as

$$k \frac{\partial T}{\partial s} \cdot n = -h(T - T_a), \quad (28)$$

where  $(k)$  is thermal conductivity,  $(T)$  is the unknown temperature,  $(n)$  is the unit vector normal to the boundary  $(S)$ ,  $(T_a)$  is ambient temperature, and  $(h)$  is the convection coefficient, which is dependent on the geometry and material properties of the heated body, as well as the velocity and material properties of the fluid present at the boundary. Heat transfer by radiation is defined as

$$k \frac{\partial T}{\partial s} \cdot n = \epsilon \gamma (T^4 - T_a^4), \quad (29)$$

where  $(\epsilon)$  is the emissivity of the heated body, and  $(\gamma)$  is the Stefan-Boltzmann constant.

After solving for the unknown temperature  $(T)$  at time  $(t)$ , heat flux  $(\vec{\phi}_q)$  can be calculated with Fourier's Law.

$$\vec{\phi}_q = -k \nabla T \quad (30)$$



## Chapter 4: Numerical Modeling

### 4.1 Limitation of Scope

For practical reasons, the scope of problems modeled in this study has been limited. At the current level of development, interest is placed on thermal evolution in the heated bodies near the induction coil without regard to the motion required in the process. Although the process for modeling nonlinear materials will be described, implementation within the modeling algorithms has been left for future work. This is reasonable since aluminum alloys are the primary materials in the study and they have a relative permeability of  $\sim 1.0$ , making them paramagnetic, and hysteresis is not a concern. Furthermore, ferromagnetic materials undergo considerable changes in magnetic properties above the Curie temperature [15,16], requiring additional complexity in the coupled electro-thermal problem. As will be shown, when a sinusoidal current source is used and the problem space is limited to linear materials (or materials that can be treated as linear within the problem), a steady state frequency domain approach can be taken for solving the electromagnetic problem [3]. This is advantageous in that a time domain approach would require a time-stepping scheme similar to what is used in the thermodynamic portion of the problem but on a much smaller time scale. The inclusion of nonlinear materials in the electromagnetic problem also requires an iterative procedure such as successive approximation or the Newton-Raphson method to determine a new relative permeability value throughout the material for each time step, adding significant processing overhead and simulation time [3,13]. Ultimately, the thermal evolution of the body being heated is of greatest importance for the described application. With a frequency domain approach, the electromagnetic problem can be solved once to determine the heating source within the heated body, and a time-stepping scheme is then employed to simulate thermal evolution. This leads to another limiting factor in the modeling algorithms. Electrical conductivity of a material is known to be dependent on temperature. If the change in temperature is small within the problem domain, a linear approximation may be used to calculate the new conductivity. This is clearly not a viable option since temperatures are expected to range from room temperature to over 650 C, or even higher depending on melting point of the metal being heated. Furthermore, linear approximations rely on temperature coefficients based on a reference temperature, typically room temperature, further

limiting their use to a narrow range of study. Calculating changes in conductivity over large temperature ranges is a difficult problem analytically and is often avoided in favor of interpolated values from a look-up table. Such tables covering the desired temperature ranges for the specific alloy under study are difficult to find in literature, and as a result, must often be created from experimental data. Creation of temperature dependent conductivity tables has been left as future work. For similar reasons, thermal conductivity and specific heat capacity, which are dependent on temperature, are made constant in this study. For the thermodynamic problem, convection and radiation are not considered at this level of development. Their inclusion will be important in modeling the fully matured system, where heating of peripheral components in the system must be understood. Electrodynamic forces, which result in vibration and repulsion (or attraction in the case of ferromagnetic materials) between the induction coil and nearby conductive bodies, are not considered to be a primary concern at this level of development as the induction coil and substrate are held firmly in place and the aluminum filament used in experiments thus far has not exhibited adverse behavior as a result of the forces. Furthermore, the induction coil designs under consideration are rigid CNC-machined coils and are resistant to longitudinal or radial compression (or tension) which can result from electrodynamic forces. As the system develops, however, it may become necessary to study these forces as accuracy and resolution may be detrimentally affected. Lastly, the basic problem being solved exhibits symmetry that can be exploited to greatly simplify the modeling with little penalty, therefore the problem has been reduced to a 2D planar simulation. A full 3D analysis will likely become necessary.

## **4.2 Numerical Method**

The advantage of an unstructured mesh makes the Finite Element Method (FEM) attractive for modeling the physical phenomenon encountered with induction heating. Since the solution to the electromagnetic and thermal problem requires solving a significantly large matrix equation, the mesh used in the FEM algorithm can be tailored to have high node density in regions where field values change rapidly and lower node density in regions of less rapid changes. If a structured grid were used, the grid resolution would be the same throughout the problem space and would have to be high enough

to provide convergent results that closely approximate the real solution. This results in excessively large matrices, limiting the method to very simple problems. Additionally, careful construction of the unstructured mesh allows for multiple problems to be modeled using the same mesh, saving considerable processing time and memory. MATLAB® was used as the primary tool to solve the Finite Element problems in this study due to its native matrix handling ability and built-in graphics capabilities. The open source program Finite Element Method Magnetics (FEMM) was used to validate basic results from the code generated in MATLAB®.

#### 4.2.1 Finite Element Analysis using the Galerkin method

Implementing the finite element method in a way that can simplistically cover a broad range of physical problems is no trivial task. Two common approaches taken are variational methods and residual methods. Variational methods require determination of a functional (specific to the physical problem) that must be minimized [3]. For simple 2D problems, these functionals are readily available in literature; however, given the complex nature of the induction heating problem in the scope of the proposed system makes the variational approach less desirable, especially considering that the modeling will likely extend to the full 3D case in future work. A better option in this case is the method of weighted residuals, and in particular, the Galerkin method. Named after Russian mathematician Boris Grigoryevich Galerkin, the method is a special case of the weighted residuals method in which the weight functions are equivalent to the shape functions [3]. A full description of the Galerkin method is beyond the scope of this thesis, but is readily found in literature. An important point to make regarding the method is the ease in which it relates the physical problem directly to matrix equations which can be solved in a computer.

A hypothetical case is now presented to summarize the process of solving partial differential equations using the weighted residual method with FEM. The following derivation leading to equation (41) is based largely on that found in [3]. Consider the following general equation.

$$\nabla \cdot (a \nabla U) + s = 0, \quad (\text{Analytical}) \tag{31}$$

where ( $U$ ) is the unknown and ( $a$ ) and ( $s$ ) are constants. The analytical solution to this equation for the unknown value ( $U$ ), subject to boundary conditions, represents an exact solution. Numerical modeling provides an approximation, so the difference between the exact and numerical solutions is considered a *residual* ( $R$ ).

$$\nabla \cdot (a \nabla U) + s = R \quad (\text{Numerical}) \quad (32)$$

The aim of weighted residuals is to minimize this residual [3]. This is done by forcing it to zero over the problem domain by

$$\int W(R) d\Omega = 0, \quad (33)$$

where ( $W$ ) is a weighting function and ( $\Omega$ ) is the problem domain. Substituting (32) into (33) yields

$$\int W(\nabla \cdot (a \nabla U) + s) d\Omega = 0. \quad (34)$$

By identity,

$$W(\nabla \cdot (a \nabla U)) = \nabla \cdot W(a \nabla U) - a \nabla U \cdot \nabla W, \quad (35)$$

and (34) becomes

$$\int \nabla \cdot W(a \nabla U) d\Omega - \int a \nabla U \cdot \nabla W d\Omega + \int W s d\Omega = 0. \quad (36)$$

In order to account for boundary conditions, the divergence theorem is utilized. The theorem states that the volume integral of the divergence of a vector function over the volume ( $V$ ) enclosed by a surface ( $S$ ) is equal to the flux of the vector function through that surface.

$$\int \nabla \cdot \vec{A} dv = \oint \vec{A} \cdot ds. \quad (37)$$

As such, the first term in (36) becomes a surface integral.

$$\oint W(a\nabla U) \cdot ds - \int a\nabla U \cdot \nabla W d\Omega + \int W s d\Omega = 0. \quad (38)$$

For the 2D case, the domain ( $\Omega$ ) is a surface, and the first term in (36) is converted to a line integral in a similar way. For both cases, only first order derivatives are used, and for this reason they are considered “weak” formulations [3]. This refers only to the order of the derivatives, and not to the strength of the method. Finite difference approximations of first order derivatives are ideal for numerical modeling, whereas second order finite differences are more tedious and can suffer in accuracy.

Now that the problem has been expressed in terms of weighted residuals, the discussion turns to transforming the problem into a matrix equation of the form

$$kU = S, \quad (39)$$

where ( $k$ ) is the stiffness matrix, ( $U$ ) is the vector of unknowns, and ( $S$ ) is the source or excitation vector. This involves separation for the terms in (38) into those that depend on the unknown quantity ( $U$ ) and those that do not. Terms that depend on the unknown will become part of the stiffness matrix, and those terms that are independent of the unknown become part of the source vector ( $S$ ). As such, (38) is rearranged as follows:

$$\oint W(a\nabla U) \cdot ds - \int a\nabla U \cdot \nabla W d\Omega = - \int W s d\Omega. \quad (40)$$

#### 4.2.2 Discretization of the problem domain

The finite element method involves discretizing the problem domain into smaller subdomains, or elements. The most common approach is to use triangular elements to discretize the domain as shown in Figures 4.1 and 4.2. Notice that the mesh has higher density in some areas. This is necessary to reach convergent results in areas where field values are expected to be rapidly changing.

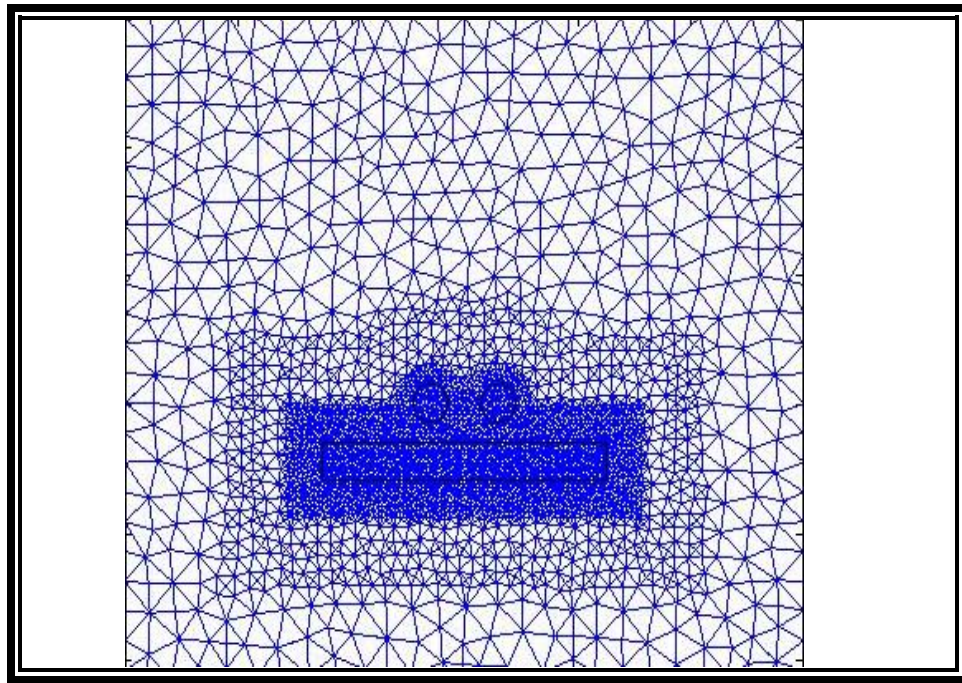


Figure 4.1: 2D Discretized problem domain.

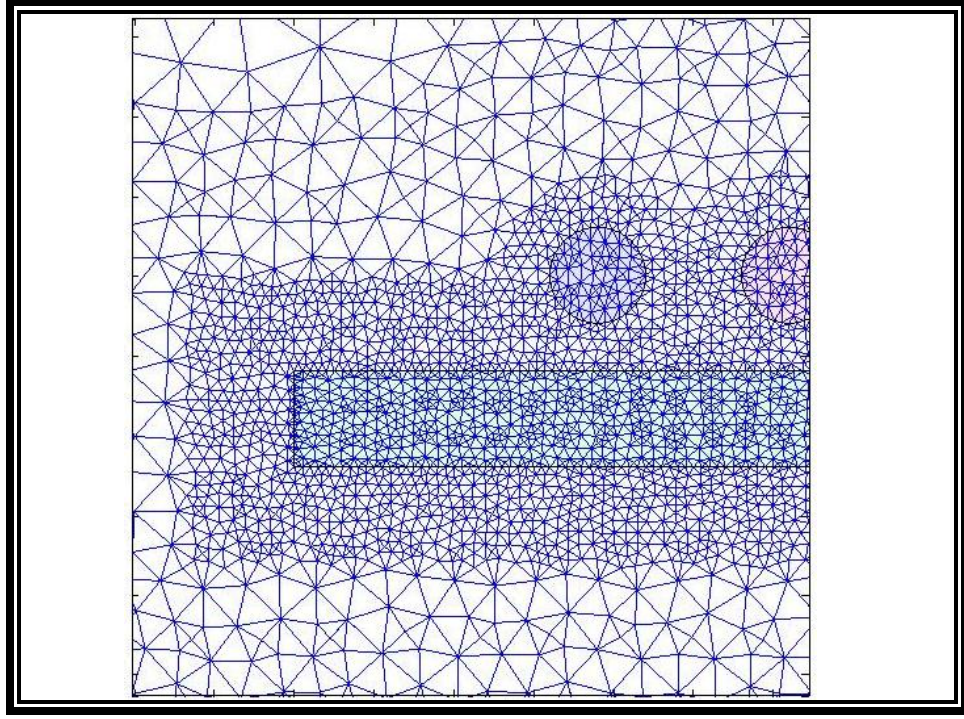


Figure 4.2: Refined mesh showing material boundaries.

Once the domain has been discretized, equation (40) can be reformulated as the sum of the integrals on each element as follows:

$$\sum_{k=1}^K \oint W(a\nabla U) \cdot ds_k - \sum_{k=1}^K \int a\nabla U \cdot \nabla W d\Omega_k = - \sum_{k=1}^K \int W s d\Omega_k \quad (41)$$

where (  $S_k$  ) is a boundary edge on the kth element (  $\Omega_k$  ), and (  $K$  ) is the total number of elements. Recall that the first term is related to boundary conditions and is not included for the summation of edges not on defined boundaries. Local integration (at the element level) of each term is accomplished with numerical integrations and finite difference approximations for the derivatives. The vertices of each element are called nodes. The order of the element determines how many nodes an element has. For example, a first order triangular element has three nodes per element, but a second order (quadratic) triangular element has six nodes, one for each vertex, and one at the midpoint between vertices on the three sides of the triangular element. Second order elements have two advantages. They provide improved accuracy over first order elements, and they can accommodate curvilinear edges on the

elements. The exact summation and finite difference schemes used for the local integration of terms in equation (41) depend on the order of element used. A detailed description for first and second order elements can be found in [3]. An important note, however, is that a change of variables is used, along with a Jacobian matrix, to allow simple mapping between coordinate systems. This greatly simplifies local integration.

#### 4.2.3 Establishment of the Global Stiffness Matrix

The local integration process establishes a local stiffness matrix and source vector. The size of the local stiffness matrix is  $n \times n$  where  $n$  is the number of nodes in the element, and the size of the source vector is  $1 \times 1$ . Each element is uniquely numbered and each node has both a local numbering and a global numbering. Local node indexing is from (1) to (3) in the case of first order elements, and (1) to (6) for a second order element. Global node indexing is from (1) to (N), the total number of nodes in the problem space. The size of the global stiffness matrix ( $k$ ) and source vector ( $S$ ) are determined by (N). The stiffness matrix is  $N \times N$  and the source vector is  $N \times 1$ . Beginning with the first element and continuing through all elements based on their index and the global indices of their nodes, local stiffness matrices and their source vectors are assembled into the global system. The result is a sparse matrix that is symmetrical and banded.

#### 4.2.3 Enforcement of Boundary Conditions

After assembly of the stiffness matrix and source vector, boundary conditions are enforced. Boundary conditions are enforced at the node level within the global system. For Dirichlet boundary conditions such as a constant temperature the entire row of the stiffness matrix corresponding to the node is zeroed, a '1' is placed in the stiffness matrix on the diagonal at  $n, n$  and the desired constant is placed in the source vector at location  $n$ . For a Neumann boundary condition, the stiffness matrix remains unchanged, but the source vector for the particular node gets overwritten with the desired value. Like Dirichlet boundaries, convection and radiation boundaries modify both the stiffness matrix and the source vector. Once boundary conditions are in place, the stiffness matrix is no longer symmetric since



the boundaries may include edges from multiple elements, and not necessarily each edge on these elements.

#### 4.2.4 Solution to the Matrix Equation and Post Processing

Having assembled the global stiffness matrix and source vector, and having enforced boundary conditions, all that remains is to solve the matrix equation for the column of unknown values ( $U$ ). There are several ways of doing so. A couple of examples are the Bi-Conjugate Gradient method and L/U decomposition. Once the system equation has been solved, post-processing involves taking results vector ( $U$ ) and calculating other quantities. For example, if equation (21) were used as our governing equation, the solution is the magnetic vector potential ( $A$ ), and post-processing would involve solving for eddy current density ( $Je$ ) throughout the domain and then the Joule heat source ( $Q$ ). If equation (27) was the governing equation, the solution is temperature ( $T$ ) throughout the problem domain, and post-processing could involve solving for heat flux ( $\vec{\phi}_q$ ). It's important to understand that the solution to the matrix equation provides solution values at the nodes. For values at arbitrary points within the domain, interpolation functions must be used. Fortunately, these interpolation functions are the same as the shape functions that are created during the local integration procedure [3]. Problems involving a time derivative, and thus a transient solution, such as the thermal problem require a time discretization and the use of finite differences for each time interval ( $dt$ ). In these types of problems, part of the derivative (the  $t + \Delta t$  term) is assembled into the global stiffness matrix, and the known value (at time  $t$ ) is assembled into the source vector. The results from an iteration are stored for use as initial values in the next iteration, and so on.

#### 4.3 Solution to the Electromagnetic Problem

The problem domain shown in Figs 4.1 and 4.2 represents a cross section of a conductive plate with a coil placed immediately above. A sinusoidal source was defined for the coil, and simulations were performed for both paramagnetic and ferromagnetic plates. The Galerkin method was applied to equation (21) to solve for the magnetic vector potential ( $A$ ). The outer boundary on the problem domain

was given Dirichlet boundary conditions and Neumann boundary conditions on successive simulations. The following figures represent results from the custom MATLAB code along with simulations from the software package Finite Element Method Magnetics (FEMM) for comparison.

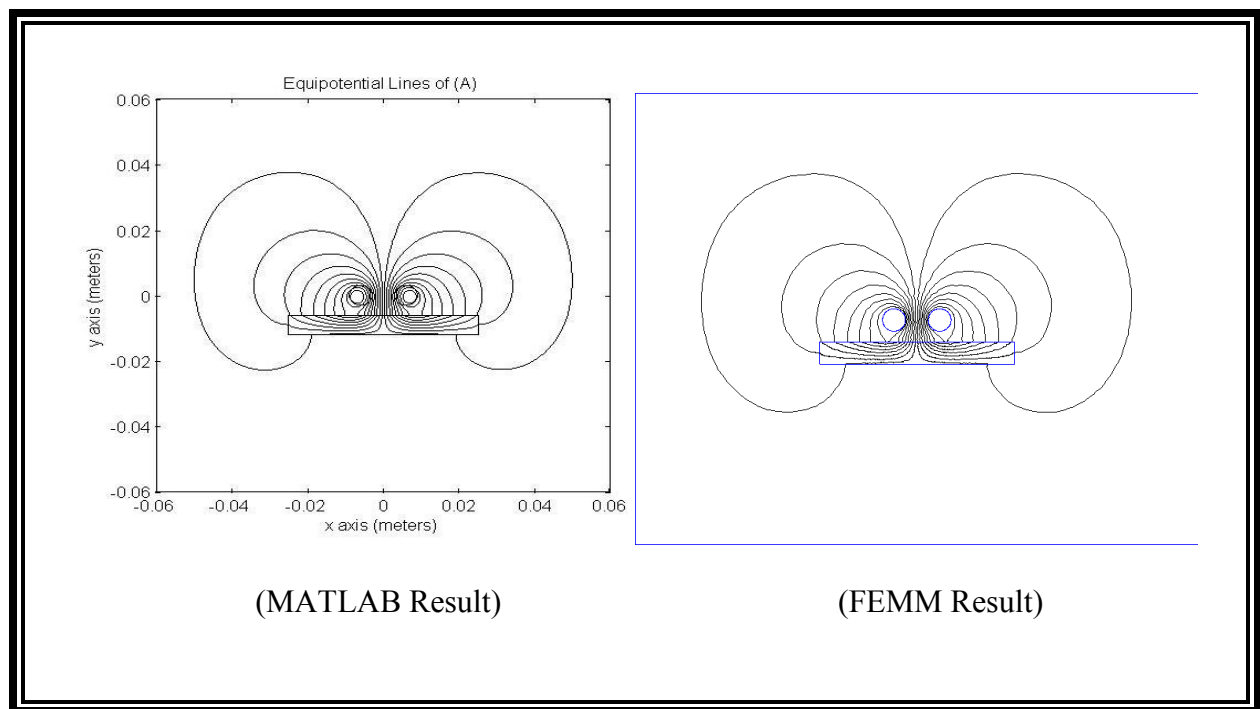


Figure 4.3: Magnetic Vector Potential with magnetic plate and Dirichlet Boundary conditions.

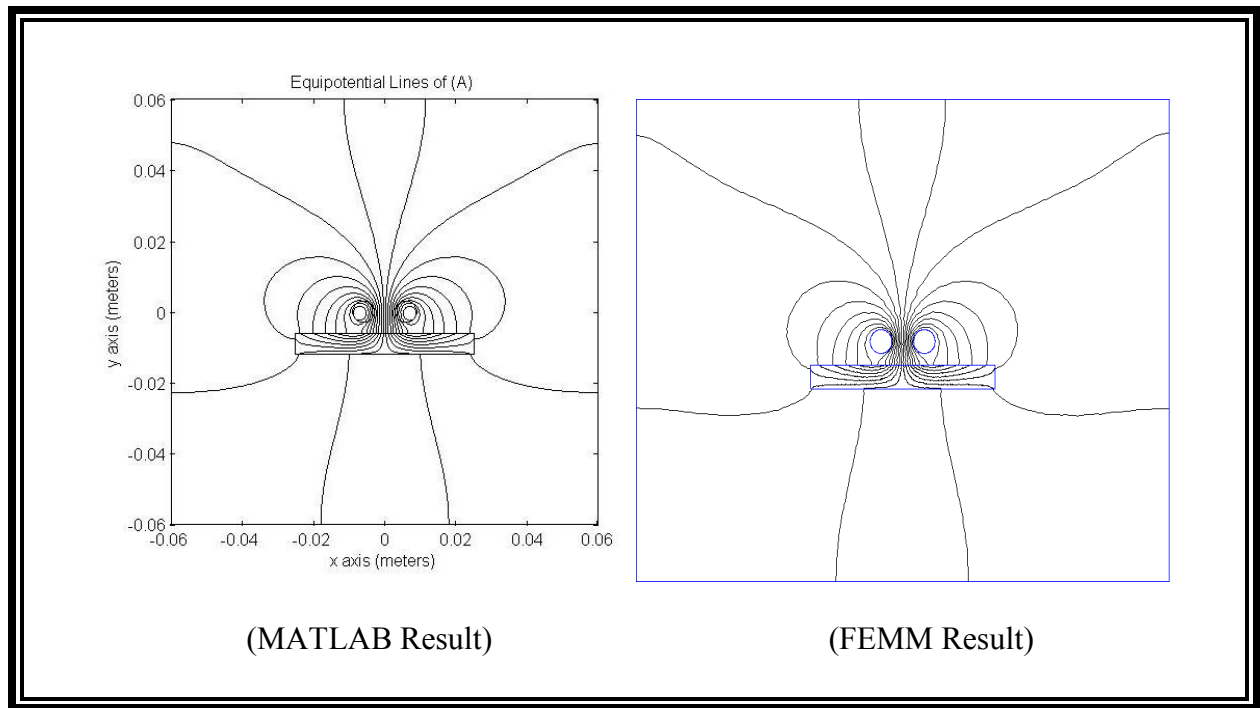


Figure 4.4: Magnetic Vector Potential with magnetic plate and Neumann Boundary conditions.

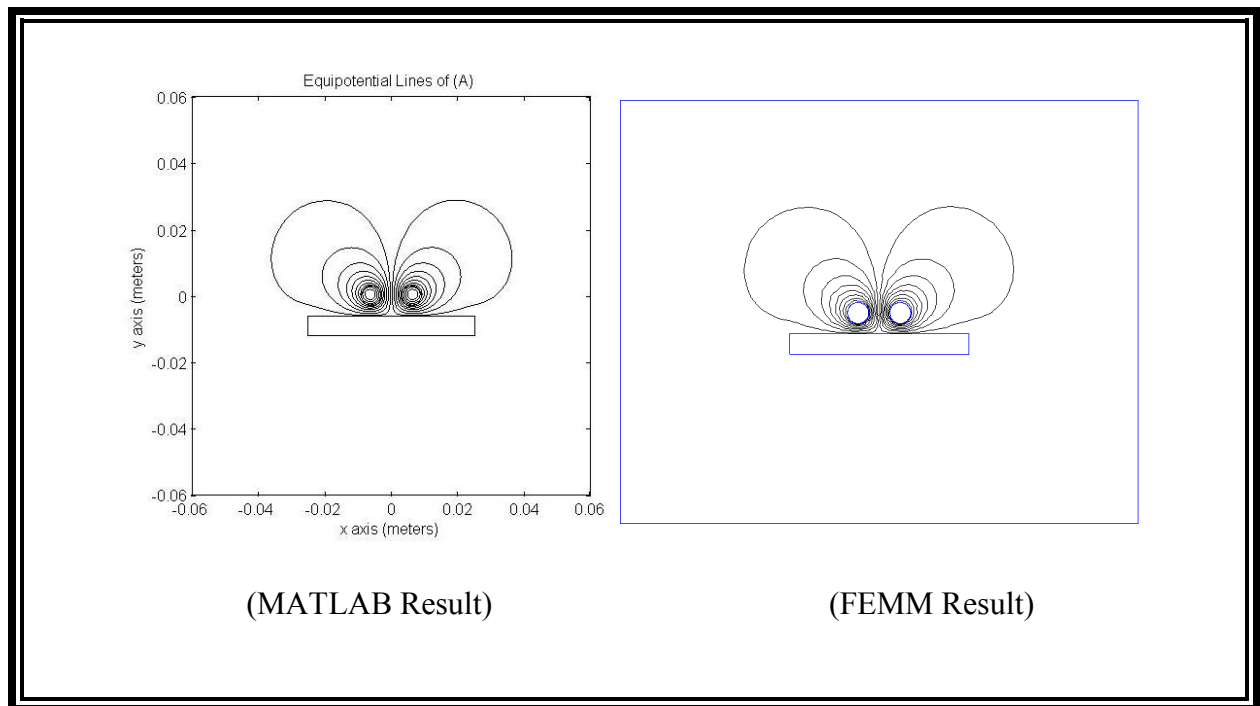


Figure 4.5: Magnetic Vector Potential with paramagnetic plate and Dirichlet Boundary conditions.

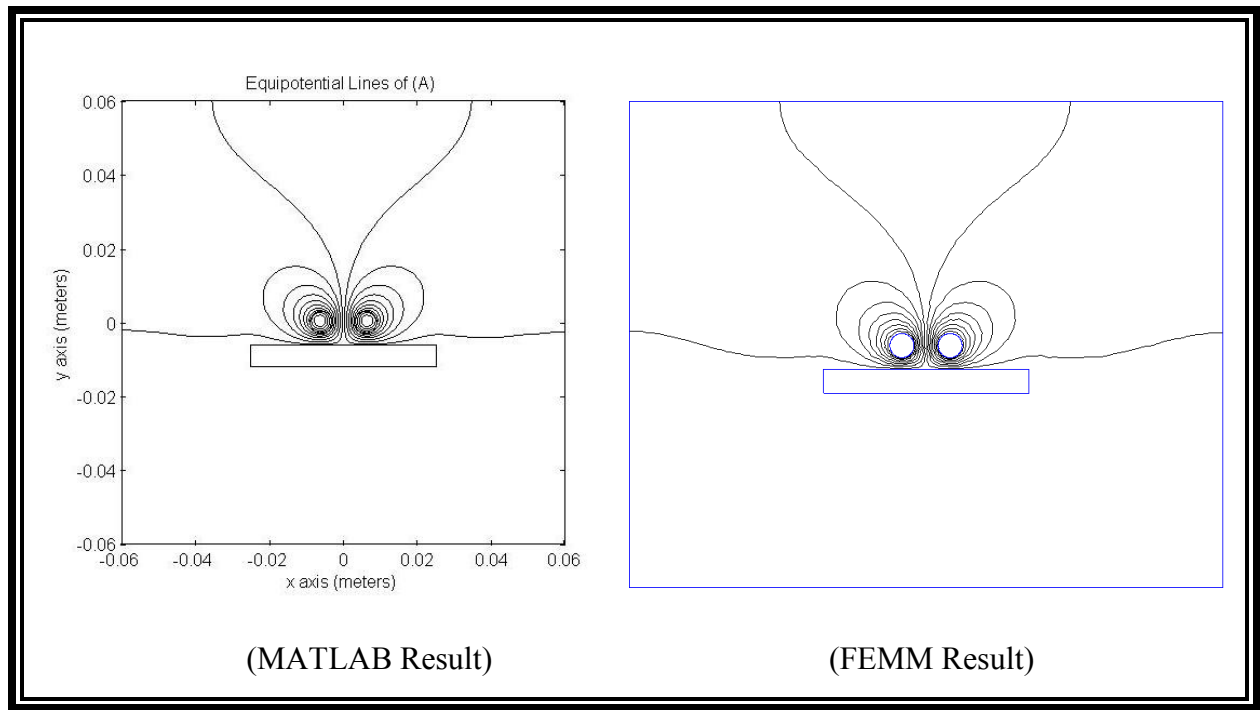


Figure 4.6: Magnetic Vector Potential with paramagnetic plate and Neumann Boundary conditions.

In looking at the electromagnetic problem, the magnetic vector potential plots are reasonably close between the MATLAB and FEMM results.

#### 4.4 Solution to the Thermodynamic Problem

As with the electromagnetic problem, the thermodynamic problem uses the mesh shown in Figs. 4.1 and 4.2, and the solution to the magnetic vector potential, using Dirichlet boundary conditions, was used to generate the heat source for the thermal simulation. The Galerkin method was applied to equation (27) and the system equation was solved for the unknown temperature ( $T$ ). The plate in this example is paramagnetic aluminum. Boundary conditions for the thermal problem included a Dirichlet condition along the outer boundary with a fixed temperature of  $27^{\circ}\text{C}$ , and another at the bottom of the plate at  $355^{\circ}\text{C}$  to simulate a controlled heating source below the plate. Radiation and convection boundaries were not used in this example. Also, only the thermal behavior of the plate is considered in this example. Initial values throughout the problem domain were set at room temperature. The plate was then allowed to heat up to a temperature of  $350^{\circ}\text{C}$  before applying the heat source from the induced

eddy currents. The figures below show the evolution of plate temperature over several intervals in time. Note that FEMM has the ability to model thermal as well as electromagnetic problems. At the time of this writing, however, it did not include a straightforward method for using the same mesh between the electromagnetic and thermal problems or for creating volumetric heat sources from the electromagnetic result. For those reasons, FEMM results for the thermodynamic problem are not shown.

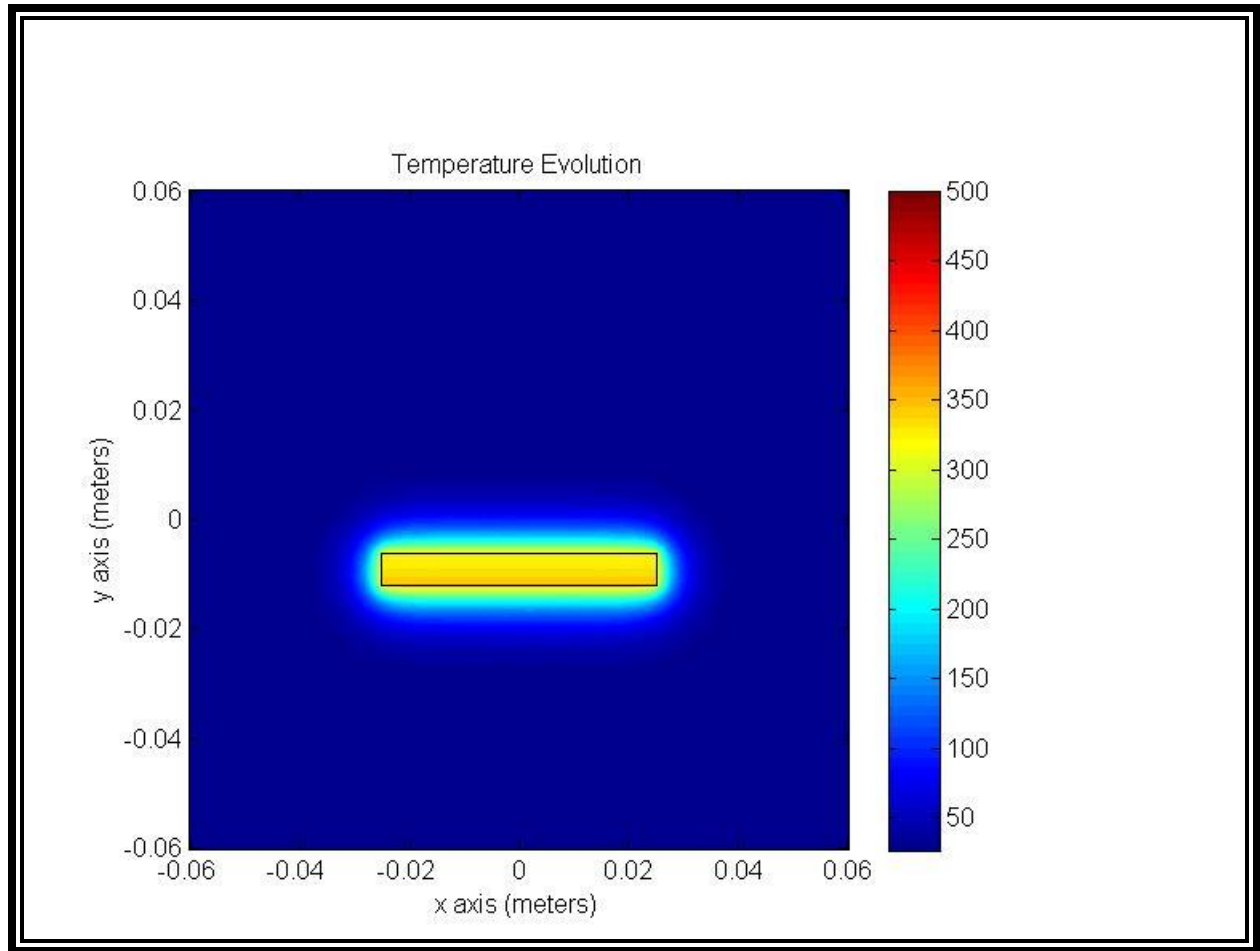


Figure 4.7: Preheated plate, no Joule Heating.

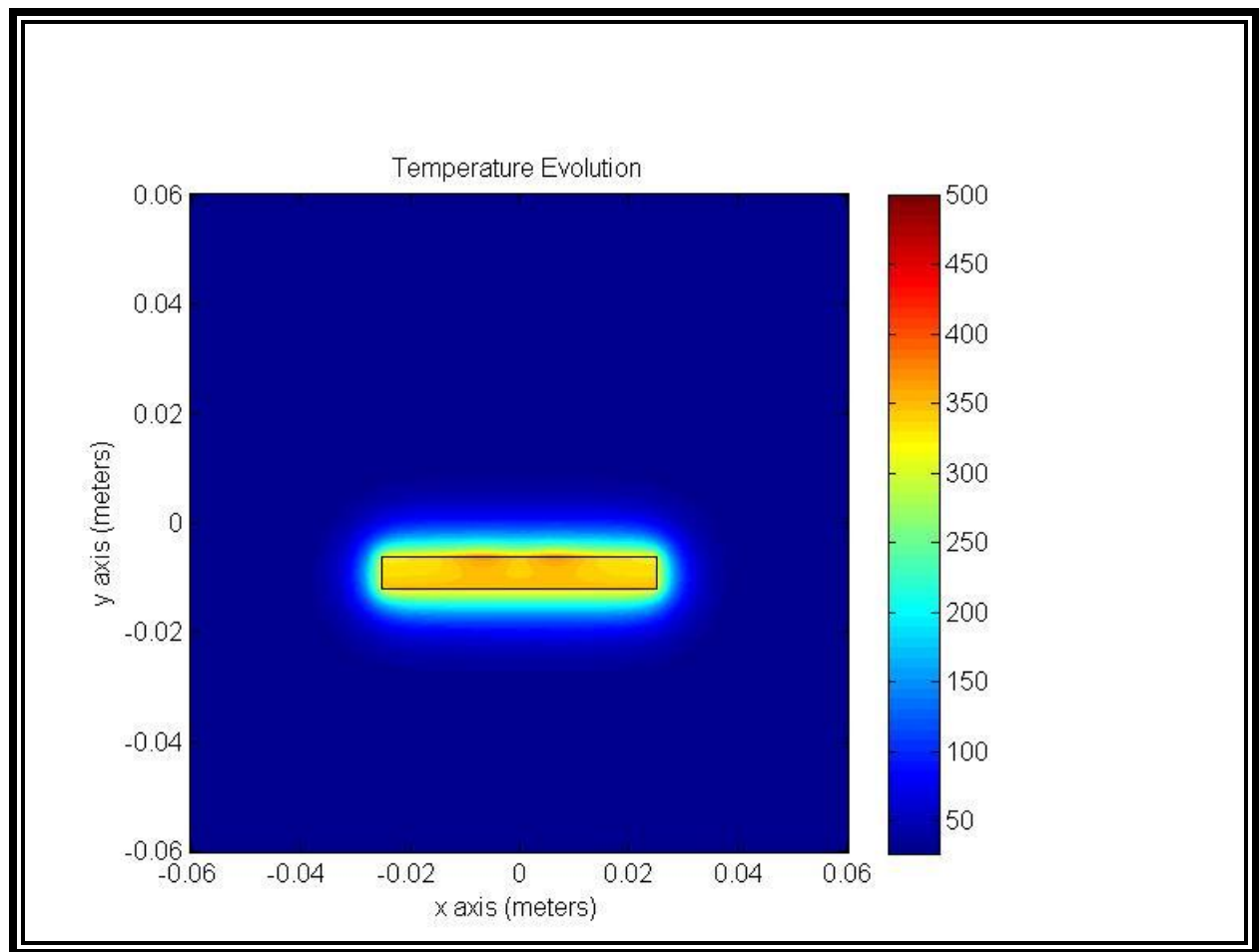


Figure 4.8: Plate heat with 2 seconds of Joule Heating.

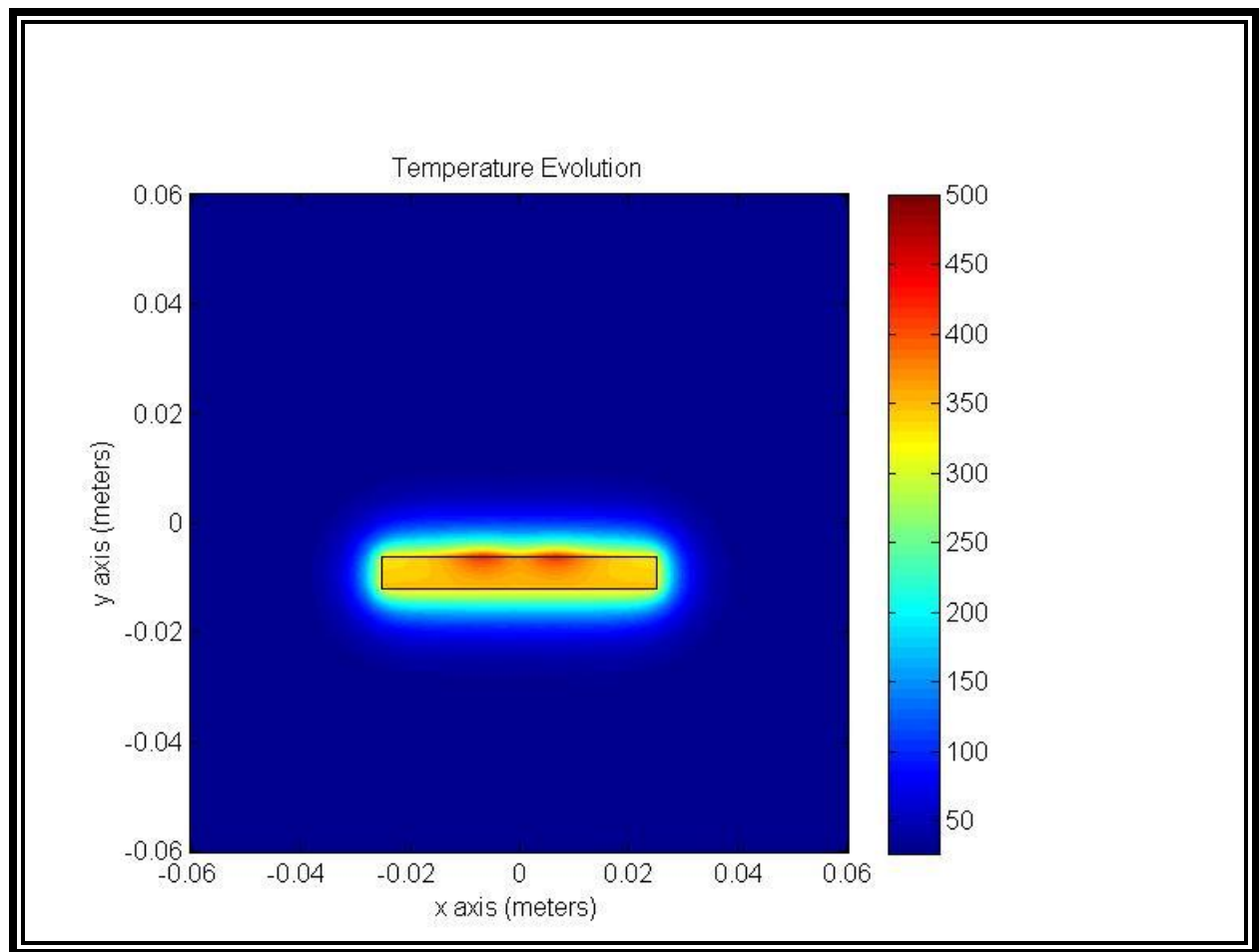


Figure 4.9: Plate heat with 5 seconds of Joule Heating.

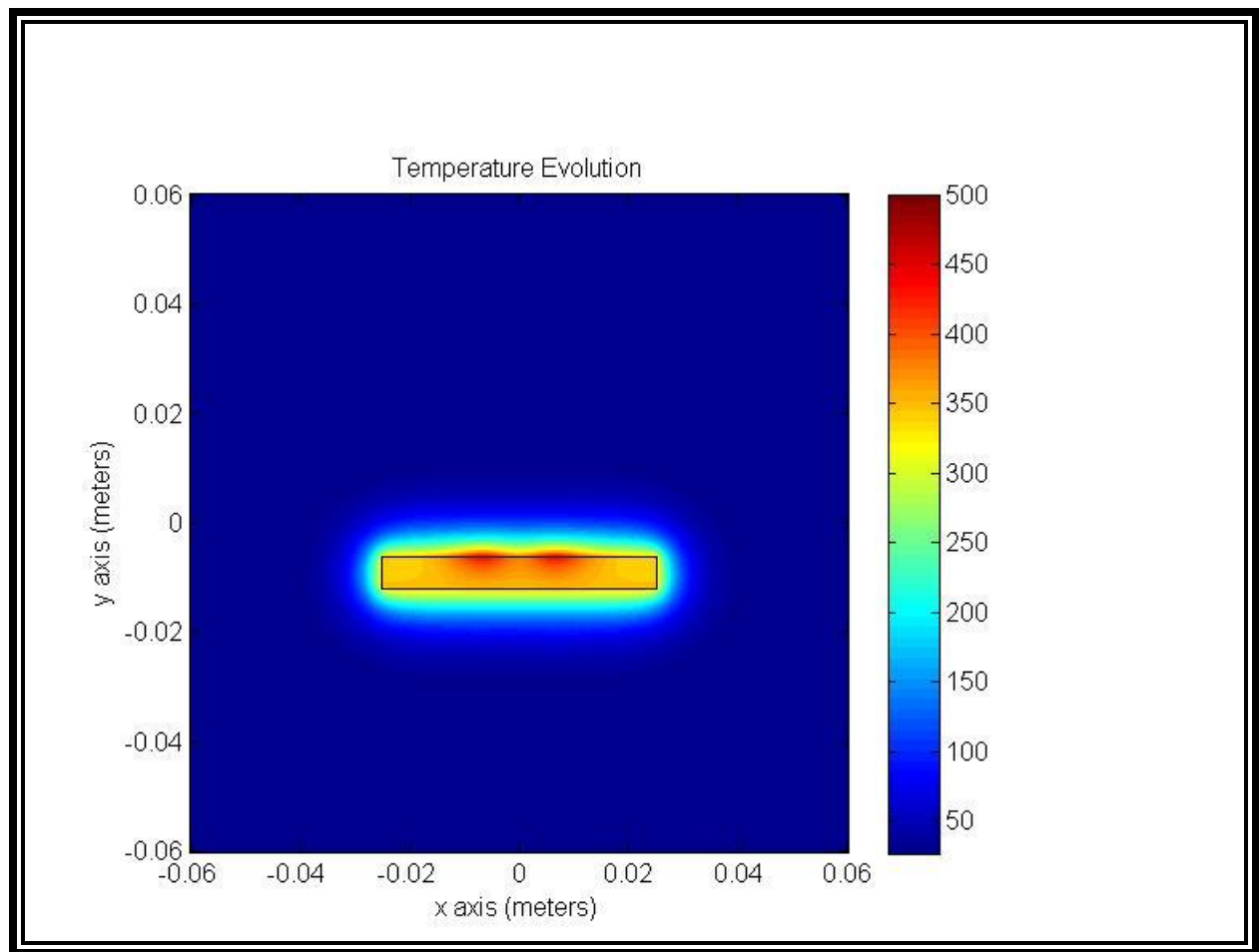


Figure 4.10: Plate heat with 8 seconds of Joule Heating.



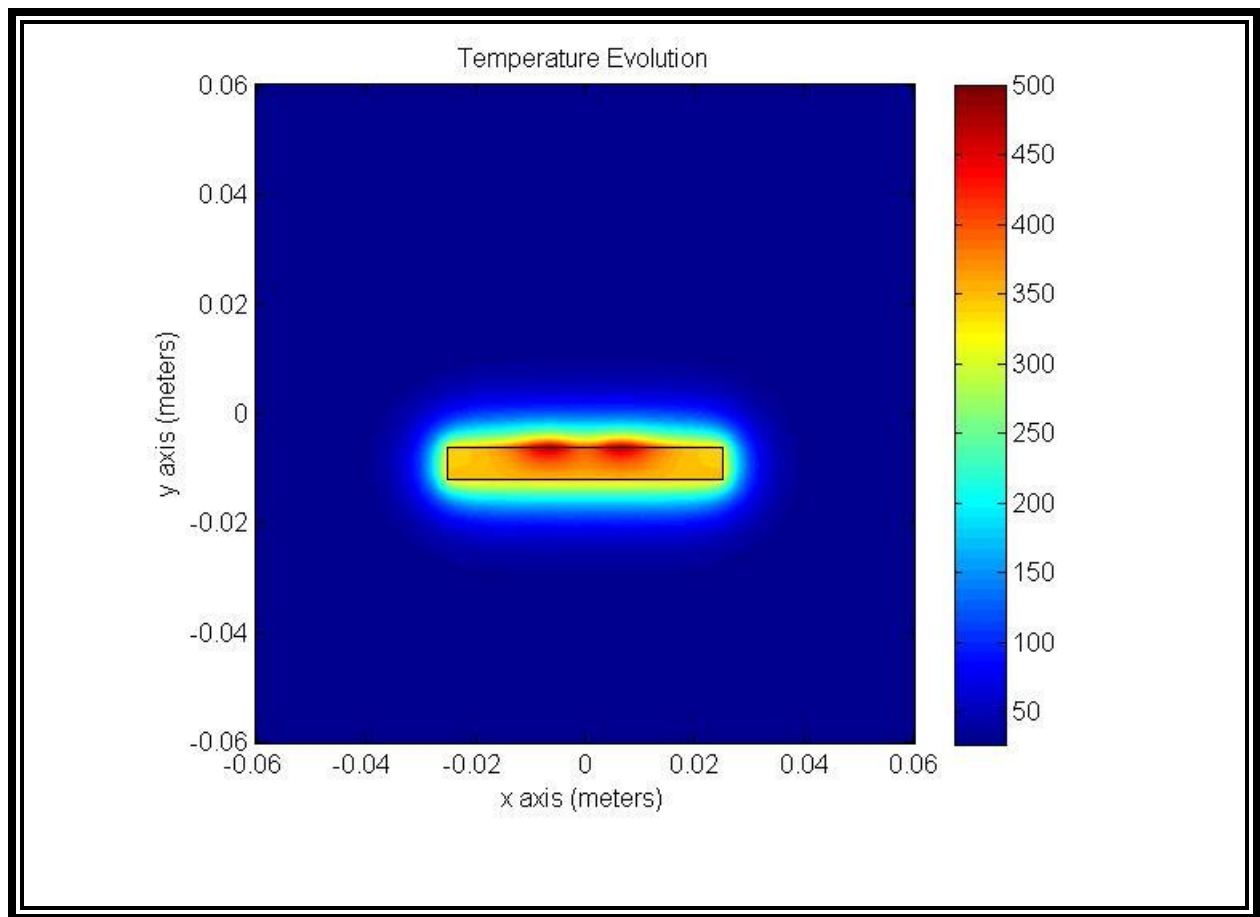


Figure 4.11: Plate heat with 10 seconds of Joule Heating.

## **Chapter 5: Initial System Design**

In this chapter, a system is proposed that makes use of induced Joule heating to heat a metal filament that is fed through an induction coil to a substrate that is also heated by the coil. The desired result is that the filament is heated to a semisolid state rather than fully molten. It is believed that deposition of the metal in this regime will be highly controllable compared to an extrusion process whereby the filament is heated beyond the melting point and then forced through a nozzle under pressure. It is anticipated that the surface upon which the semisolid metal will be deposited will need to be brought to a temperature near that of the semisolid state as well to ensure a good metallurgical bond with the new material being deposited. The rapid heating offered by induction heating is believed to be ideal for heating the surface as well as the filament being ‘wire-fed’ through the coil assembly. Basic experiments have shown that, with a high frequency (~300 kHz) induction heating system, very rapid and controllable heating of both ferromagnetic and paramagnetic metal filaments as small as 0.025” in diameter is possible. This includes the filament being fed at a rate of one centimeter per second, simulating a feed rate that might be used in a deposition process. Figure 5.1 illustrates some concepts expected to be part of the practical system.

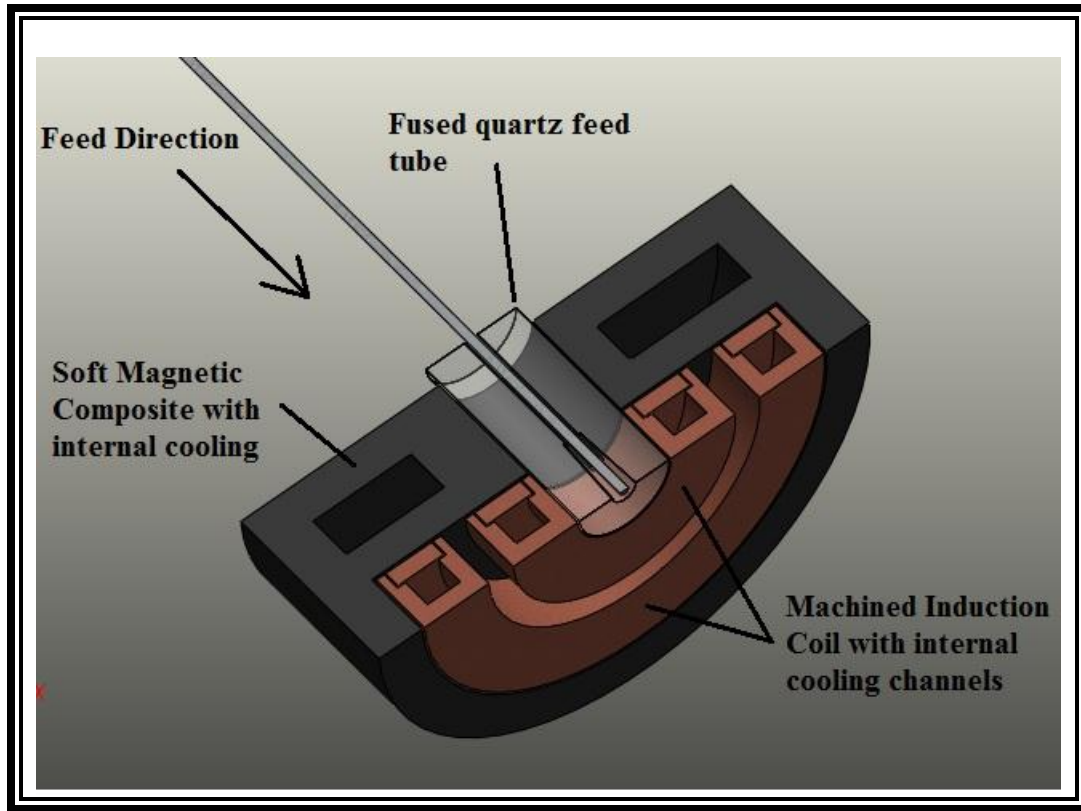


Figure 5.1: Cross-section of induction coil concept.

A multi-turn machined induction coil is shown along with a soft magnetic composite structure that will improve heating efficiency for the substrate and a fused quartz feed tube. The coil would be machined from high conductivity copper 110 which is used in high current applications for minimal loss. The quartz feed tube may serve two primary functions: 1) fused quartz can operate at sustained temperatures of up to ~1000 degrees C and is resistant to thermal shock making it ideal for guiding the metal filament through the coil and electrically insulating it; and 2) the quartz tube may be used as an optical conduit for infrared sensing, allowing noncontact temperature measurement of the deposition surface as part of the closed loop control system.

## 5.1 Off-The-Shelf Equipment

The induction power supply used in this research is a 10kW single frequency supply from Inductronix, Inc. Depending on load coil design the supply will generate alternating current from

between 200 kHz and 400 kHz with adjustable power delivered to the load of up to ~5kW. In addition to manual controls on the front panel, external control of the supply is possible through a 4-20mA control input on the back of the machine. The power supply requires a water circulator for cooling the load coil. In place is a water circulator from Dimplex Thermal Solutions, Inc. The circulator provides up to 10 gallons per minute flow rate at about 50psi for cooling the induction power supply and load coil, and it can also be used to provide cooling to peripheral components like the soft magnetic concentrator shown in Fig. 5.1. For simple experimentation, hardware from a MIG welder was adapted. The wire-feed mechanism and inert gas solenoid were used to feed metal filament through test coils at a controlled rate and provide control of the argon gas used in some tests.

To facilitate 3D layered deposition, the system will be assembled into a free-standing chassis with a build chamber. Motion control stages will be used to move a platform in the X-Y plane, and a Z stage mounted separately will control movement of the induction coil and feed mechanism. To achieve effective metal deposition with the proposed system, it would be beneficial to heat the build platform to a temperature of at least half of the melt point for the metal in use. This will complement the rapid Joule heating from the induction system by requiring only a minimal amount of additional energy to be added with induction to achieve process temperatures for deposition. As such, a heated platform will likely be part of the practical system. The build chamber will also need to be flooded with inert gas, such as argon, to prevent oxidation of the metal parts fabricated in the process, necessitating compressed argon storage and flow control.

## **5.2 Example Load Coil Design**

Several design ideas have been considered for the induction coil. Since rapid heating of the substrate (and previously deposited layers of material) to process temperatures will be done by the coil, a multi-turn planar design shows the most promise. Figures 5.2 and 5.3 show one such design. These show three nested turns joined at one end with short half-turn loops on the top of the assembly. The gap seen on each turn is minimized to allow a magnetic field to be generated that is as close to being

symmetrical as possible. This is desirable for performance that is close to that modeled with a 2D FEM program.

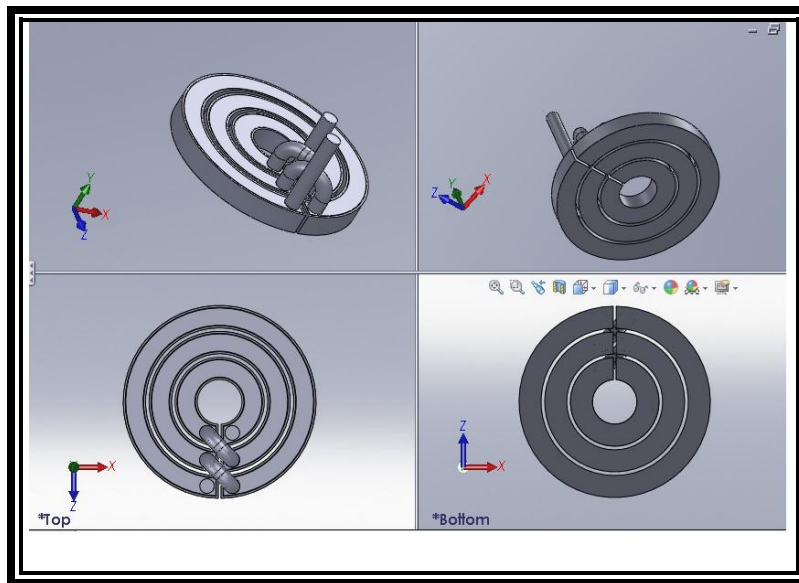


Figure 5.2: 3D model of multi-turn load coil.

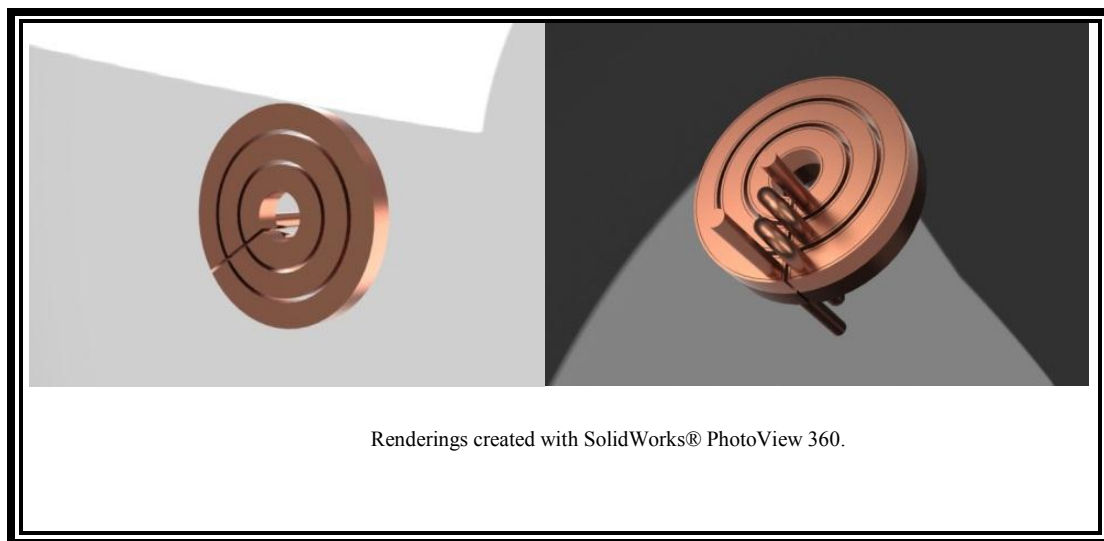


Figure 5.3: Photo Rendering of a Multi-turn Load Coil.

### 5.3 Soft Magnetic Composites

To enhance the surface heating capability of the planar induction coils, a magnetic concentrator is planned. These custom made components are made from specialized magnetic materials that have high permeability, but relatively low coercivity, meaning that hysteresis loss is minimized and flux density in the targeted areas are increased making localized induction heating more efficient. Figures 5.4 and 5.5 show a concentrator designed to work with the planar coils above.



Figure 5.4: Photo rendering of custom concentrator.

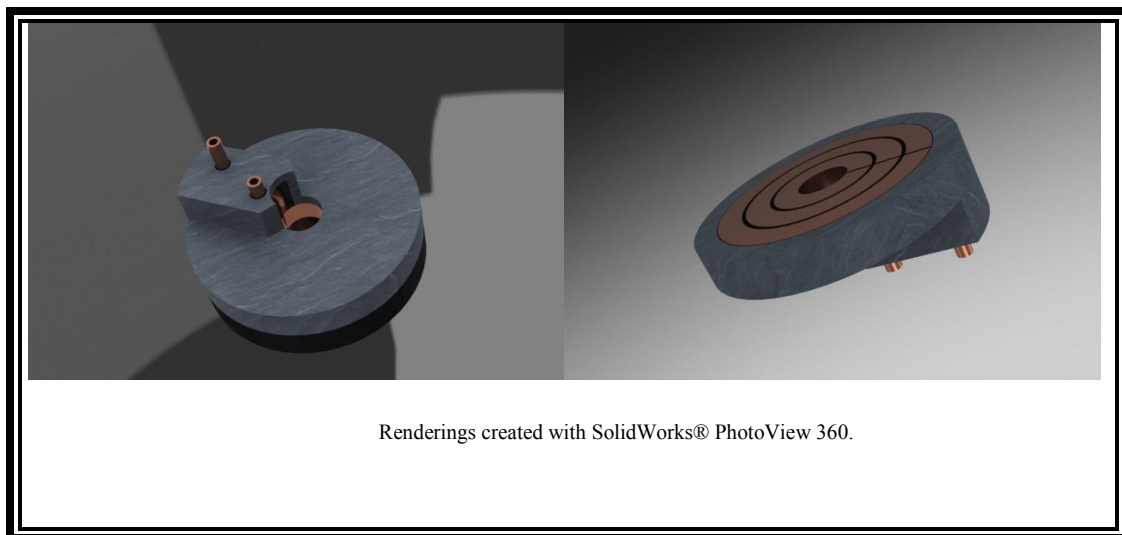


Figure 5.5: Induction Coil with integrated concentrator.

## 5.4 Coil Fabrication

The following images show machined parts and assembly of an initial test coil. Machining is done on a 5-axis CNC machine based on a SolidWorks model. Once machining is complete, the parts must be brazed together. The best method found to do this is with an induction heating system. The rapid heating allows the brazing process to occur quickly, minimizing oxidation compared to other processes.

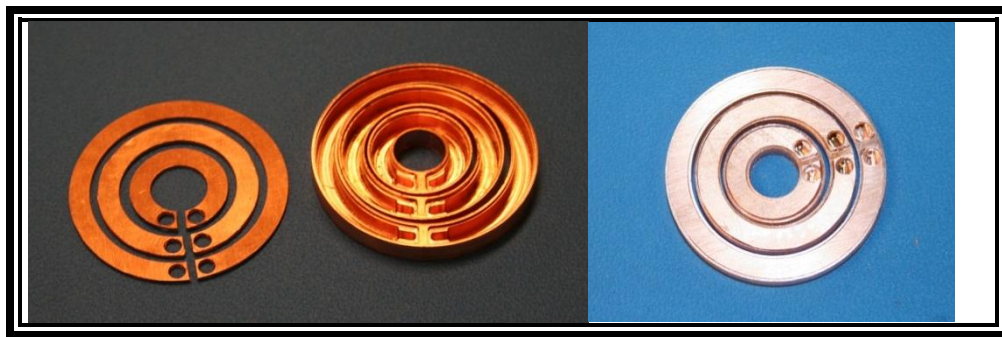


Figure 5.6: Copper load coil parts after CNC process.

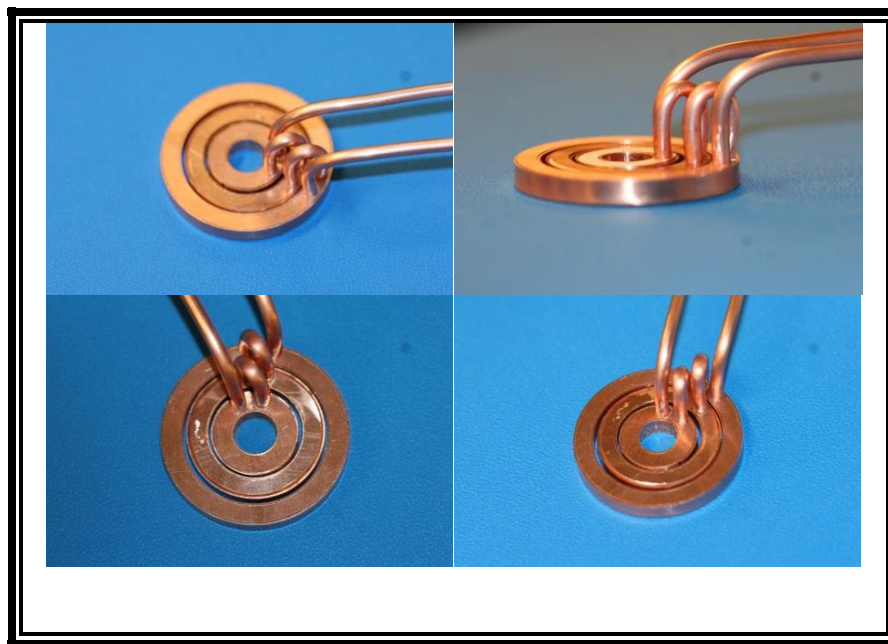


Figure 5.7: Coil Assembly before brazing.

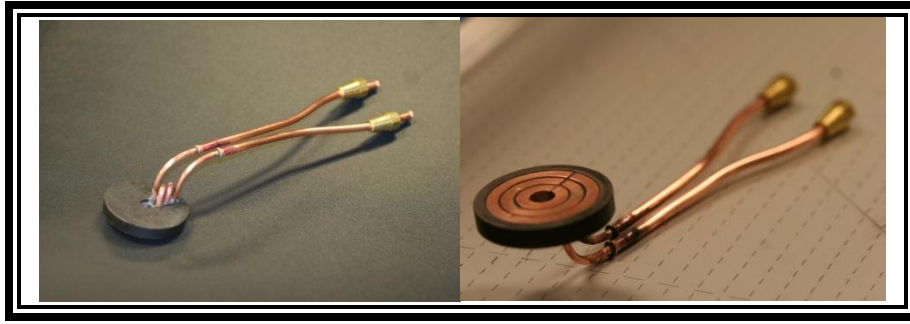


Figure 5.8: Completed test coil with concentrator.

#### 5.4 Control System

It is inevitable that closed loop control will be necessary for the practical system. In addition to precision motion and wire-feed controls, control of temperature at the maximum heat zone in the process will be critical. Thermocouples are likely to be problematic in close proximity to the induction coil. As previously mentioned, one approach might be to utilize the fused quartz tube as an optical conduit for temperature sensing of the surface. An infrared sensor could be optically coupled to the top of the quartz tube, away from intense magnetic fields and shielded from heat. Adjustable temperature control for the build platform will aid in process refinement. Output from the control system will include drive signals to the induction power supply for control of output power. Other possible outputs may be variable flow control of the inert gas and coolant circulation systems.



## **Chapter 6: Future Work**

The proposed system represents significant challenges in modeling, design, and control. Success in a practical system will require more comprehensive modeling, experimentation with quantitative results, a better understanding of the material science involved in the process, and a cost-conscious design approach. As mentioned early in this thesis, a low cost alternative to the state-of-the-art additive metals machines is needed. The proposed system is not intended to compete on a performance basis with the existing technologies, but to make the additive manufacturing of metals accessible to a much greater market with a lower cost system that provides performance that is appropriate for a large number of applications. This will require efforts to make the system compatible with a wide range of operating temperatures and materials.

### **6.1 Numerical Modeling of the Coupled Electro-thermal Phenomenon**

While working finite element code was developed for the basic electromagnetic and thermal problem, it does not take into account temperature-dependent or nonlinear material properties. Code for the electromagnetic problem must be extended with time discretization to allow for dynamic change of material properties as temperatures evolve, and to allow realistic numerical treatment of magnetic materials. Furthermore, the processing of ferromagnetic metals will require the temperature dependency of magnetic permeability and the shift magnetic properties above Curie temperature be accounted for. Code for the thermal problem must also be extended to take into account the temperature dependency of heat capacity and thermal conductivity. Implementation of convection and radiation boundaries must be completed as the effects will be an important consideration in the practical system.

Other physical phenomena may impact the performance of the proposed system and must be considered. Electrodynamic forces as a result of the intense resonant magnetic fields cause tension, compression, and vibration in the system. Ramifications of these forces must be understood early in the development of the system and numerical modeling may be justified. As a final note on modeling, the motion of the filament as it's fed in the deposition process, as well as motion of the platform relative to the induction coil assembly, must be considered in modeling of both the electromagnetic and thermal

processes. Several examples exist in literature for adapting the finite element method for both linear and rotary motion within the problem domain.

## **6.2 Experimentation**

Little has been done in the way of experimentation for the proposed system. What has been observed is promising, but has been more qualitative than quantitative. While modeling is critical to understanding the physical phenomena involved with the system, experimentation is needed to validate the numerical results and ensure the behavior of major system components are effective. Progressive demonstrations of the system are planned with quantitative results being a priority.

## **6.3 Material Science**

A better understanding of the material science involved in the proposed system is important for many reasons. Metal parts fabricated in the system will have a wide range of applications and the mechanical performance resulting from the raw materials and the process must be known. This will require knowledge of composition of the alloys used, phase diagrams, and microstructure resulting from the induction heating and deposition process. Selection and process development for each alloy adapted for use in the system will begin with material science. Aside from the parts fabricated, material for system components will be chosen based on the ability to endure the high temperature, intense electromagnetic environment for extended periods of time. Success of the system depends on durability of such components.

## References

- [1] V. Rudnev, D. Loveless, R. Cook, M. Black, "Handbook of Induction Heating." New York, NY: Marcel Dekker, Inc., 2003.
- [2] A. Mühlbauer, "History of Induction Heating & Melting." Essen Germany: Vulkan-Verlag GmbH, 2008.
- [3] J.P.A. Bastos, N. Sadowski, "Electromagnetic Modeling by Finite Element Methods", New York, NY: Marcel Dekker, Inc., 2003.
- [4] N. Kipnis, "Chance in Science: The Discovery of Electromagnetism by H.C. Oersted." *Science and Education*, no. 14, pp. 1-28, 2005.
- [5] P. Hammond, "Andre-Marie Ampere: the Newton of electricity." *Journal of the Institution of Electrical Engineers*, vol. 77, pp. 274-277, May 1961.
- [6] M. Kranjc, A. Zupanic, D. Miklavcic, T. Jarm, "Numerical Analysis and Thermographic Investigation of Induction Heating." *International Journal of Heat and Mass Transfer*, no 53, pp. 3585-3591, April 2010.
- [7] M.H. Tavakoli, H. Karbaschi, and F. Samavat, "Computational Modeling of Induction Heating Process." *Progress In Electromagnetics Research Letters*, vol. 11, pp. 93-102, 2009.
- [8] J. Nerg, J. Partanen, "Numerical Solution of 2D and 3D Induction Heating Problems with Non-Linear Material Properties Taken into Account." *IEEE Transactions on Magnetics*, vol. 36, no. 5, pp. 3119-3121, Sept 2000.
- [9] L.R. Egan, E.P. Furlani, "A Computer Simulation of an Induction Heating System." *IEEE Transactions on Magnetics*, vol. 27, no. 5, pp. 4343-4354, Sept 1991.
- [10] C. Chaboudez, S. Clain, R. Glardon, D. Mari, J. Rappaz, M. Swierkosz, "Numerical Modeling in Induction Heating for Axisymmetric Geometries." *IEEE Transactions on Magnetics*, vol. 33, no. 1, pp. 739-745, Jan 1997
- [11] C.G. Kang, P.K. Seo, H.K. Jung, "Numerical Analysis by New Proposed Coil Design Method in Induction Heating Process for Semi-Solid Forming and its Experimental Verification with Globalization Evaluation." *Material Science and Engineering*, A341, pp. 121-138, 2003.
- [12] F. Bay, V. Labbe, Y. Favennec, J. L. Chenot, "A Numerical Model for Induction Heating Process Coupling Electromagnetism and Thermomechanics." *International Journal for Numerical Methods in Engineering*, n0. 58, pp. 839-867, Jan 2003.
- [13] P.K. Vong, D. Rodger, "Coupled Electromagnetic-Thermal Modeling of Electrical Machines." *IEEE Transactions on Magnetics*, vol. 39, no. 3, pp. 1614-1617, May 2003.
- [14] J. Nerg, J. Partanen, "A Simplified FEM based Calculation Model for 3-D Induction Heating Problems Using Surface Impedance Formulations." *IEEE Transactions on Magnetics*, vol. 37, no. 5, pp. 3719-3722, Sept 2001.
- [15] M. Enokizono, H. Tanabe, "Numerical Analysis of High-Frequency Induction Heating Including Temperature Dependence of Material Characteristics." *IEEE Transactions on Magnetics*, vol. 31, no. 4, pp. 2438-2444, July 1995.
- [16] B. Drobenko, O. Hachkevych, T. Kournyts'kyi. "A Mathematical Simulation of High Temperature Induction Heating of Electroconductive Solids." *International Journal of Heat and Mass Transfer*, no 50, pp. 616-624, 2007.

## **Vita**

Danny Muse was born in Meridian, Mississippi. He graduated from Clarkdale High School, in Meridian in the spring of 1986, after which he entered the United States Air Force and studied electronics and radar systems. After leaving the military, he entered the world of commercial electronics and manufacturing. While working in various technical and managerial roles in the electronics and manufacturing industries, he also attended community colleges in Abilene, Texas and Aptos, California, to complete lower level courses in preparation for university studies in engineering. After about a 12 year break in courses, He returned to school at El Paso Community College and the University of Texas at El Paso. He graduated summa cum laude on December, 2009 with the Bachelor of Science in Electrical Engineering from the University of Texas at El Paso. While completing studies at UTEP, he worked as a research associate and program coordinator in the W. M. Keck Center for 3D Innovation, where he developed an interest in additive manufacturing technologies. In the spring of 2010, he entered Graduate School at the University of Texas at El Paso. Continuing to work in the Keck Center, he plans to further his education with a doctoral program in Material Science and Engineering.

Permanent address: 4125 River Bend Drive  
El Paso, Texas, 79922

This thesis/dissertation was typed by Danny Wayne Muse.